Progress in Oceanography 197 (2021) 102653

Contents lists available at ScienceDirect

Progress in Oceanography

journal homepage: www.elsevier.com/locate/pocean

Environment, ecology, and potential effectiveness of an area protected from deep-sea mining (Clarion Clipperton Zone, abyssal Pacific)

Daniel O.B. Jones [a,*], Erik Simon-Lledó [a], Diva J. Amon [b], Brian J. Bett [a], Clémence Caulle [c], Louis Clément [a], Douglas P. Connelly [a], Thomas G. Dahlgren [d,e], Jennifer M. Durden [a], Jeffrey C. Drazen [f], Janine Felden [g], Andrew R. Gates [a], Magdalena N. Georgieva [b], Adrian G. Glover [b], Andrew J. Gooday [a,b], Anita L. Hollingsworth [a,h], Tammy Horton [a], Rachael H. James [h], Rachel M. Jeffreys [i], Claire Laguionie-Marchais [j], Astrid B. Leitner [k], Anna Lichtschlag [a], Amaya Menendez [h], Gordon L.J. Paterson [b], Kate Peel [a], Katleen Robert [l], Timm Schoening [m], Natalia A. Shulga [n], Craig R. Smith [f], Sergio Taboada [b,o,p], Andreas M. Thurnherr [q], Helena Wiklund [b,e], C. Robert Young [a], Veerle A.I. Huvenne [a]

[a] National Oceanography Centre, European Way, Southampton SO14 3ZH, UK
[b] Life Sciences Department, Natural History Museum, Cromwell Rd, London SW7 5BD, UK
[c] Ocean Zoom, Nantes 44200 / Brest 29200, France
[d] NORCE, Postboks 22 Nygårdstangen, 5838 Bergen, Norway
[e] Gothenburg Global Biodiversity Centre and Department of Marine Sciences, University of Gothenburg, 40530 Gothenburg, Sweden
[f] University of Hawai'i at Manoa, Department of Oceanography, 1000 Pope Rd, Honolulu, HI 96821, USA
[g] MARUM – Center for Marine Environmental Sciences, University of Bremen, Leobener Str. 8, D-28359 Bremen, Germany
[h] Ocean and Earth Science, University of Southampton, National Oceanography Centre Southampton, University of Southampton Waterfront Campus, European Way, Southampton SO14 3ZH, UK
[i] School of Environmental Sciences, University of Liverpool, Liverpool, UK
[j] Ryan Institute, & School of Natural Sciences, Zoology, NUI Galway, University Road, Galway, Ireland
[k] Monterey Bay Aquarium Research Institute, 7700 Sandholdt Rd, Moss Landing, CA 95039, USA
[l] Fisheries and Marine Institute of Memorial University of Newfoundland, Canada
[m] Deep Sea Monitoring Group, GEOMAR Helmholtz Center for Ocean Research, Kiel, Germany
[n] Shirshov Institute of Oceanology, Russian Academy of Sciences, Moscow, Russia
[o] Departamento de Biodiversidad, Ecología y Evolución, Universidad Complutense de Madrid, Madrid, Spain
[p] Departamento de Ciencias de la Vida, Universidad de Alcalá de Henares, Madrid, Spain
[q] Lamont-Doherty Earth Observatory, Palisades, NY, 10964-8000, USA

ARTICLE INFO

Keywords:
Area of Particular Environmental Interest
APEI-6
Environmental Management
Baseline
Clarion-Clipperton Zone
Polymetallic nodules
Ocean conservation
Marine protected area

ABSTRACT

To protect the range of habitats, species, and ecosystem functions in the Clarion Clipperton Zone (CCZ), a region of interest for deep-sea polymetallic nodule mining in the Pacific, nine Areas of Particular Environmental Interest (APEIs) have been designated by the International Seabed Authority (ISA). The APEIs are remote, rarely visited and poorly understood. Here we present and synthesise all available observations made at APEI-6, the most north eastern APEI in the network, and assess its representativity of mining contract areas in the eastern CCZ. The two studied regions of APEI-6 have a variable morphology, typical of the CCZ, with hills, plains and occasional seamounts. The seafloor is predominantly covered by fine-grained sediments, and includes small but abundant polymetallic nodules, as well as exposed bedrock. The oceanographic parameters investigated appear broadly similar across the region although some differences in deep-water mass separation were evident between APEI-6 and some contract areas. Sediment biogeochemistry is broadly similar across the area in the parameters investigated, except for oxygen penetration depth, which reached >2 m at the study sites within APEI-6, deeper than that found at UK1 and GSR contract areas. The ecology of study sites in APEI-6 differs from that reported from UK1 and TOML-D contract areas, with differences in community composition of microbes, macrofauna, xenophyophores and metazoan megafauna. Some species were shared between areas although connectivity appears

* Corresponding author.
E-mail address: dj1@noc.ac.uk (D.O.B. Jones).

https://doi.org/10.1016/j.pocean.2021.102653
Received 28 January 2021; Received in revised form 17 June 2021; Accepted 14 July 2021
Available online 21 July 2021

limited. We show that, from the available information, APEI-6 is partially representative of the exploration areas to the south yet is distinctly different in several key characteristics. As a result, additional APEIs may be warranted and caution may need to be taken in relying on the APEI network alone for conservation, with other management activities required to help mitigate the impacts of mining in the CCZ.

1. Introduction

The Clarion-Clipperton Zone (CCZ) is a seabed area of approximately 6 million km^2, receiving scientific and commercial interest for its vast resources of polymetallic nodules (Lodge et al., 2014). The CCZ is situated in the eastern Pacific between the Clarion and Clipperton fracture zones stretching from 5° to 20° N and 115 to 160° W and covers over 1% of the world's surface. There has been a long history of scientific and industrial exploration of this area. Nodules were first discovered close to the CCZ by the 1872–1876 HMS *Challenger* expedition (Murray and Renard, 1891). The first studies of potential mining impacts were carried out here in the 1970s (reviewed in Jones et al., 2017) but commercial exploitation has not yet occurred. As the CCZ is predominantly seabed beyond national jurisdiction, the mineral resources are regulated by the International Seabed Authority (ISA). The ISA has divided the CCZ into various mining exploration contract areas assigned to state-sponsored contractors. In addition, the ISA has produced a spatial management plan for the CCZ that includes nine Areas of Particular Environmental Interest (APEIs), with original locations designed to be areas representative of the region expected to sustain mining impacts (Wedding et al., 2013). The original design of APEIs was based on modelled information on environmental characteristics, such as food supply based on particulate organic carbon flux (Smith et al., 2008), nodule density, seabed morphology, together with expert opinion. In addition, the locations of existing and emerging exploration contracts were taken into account (Wedding et al., 2013). Two of the APEIs were moved by the ISA from the central area, with the area now designated as APEI-6 moved to the northeast corner of the CCZ (Wedding et al., 2013). Importantly, so far there has been limited scientific research within the APEIs and the seafloor ecosystems in several have not been sampled or studied (Laroche et al., 2020; Leitner et al., 2017; Simon-Lledó et al., 2019a; Vanreusel et al., 2016; Washburn et al., 2021). For example, the recent Friday Harbor workshop (International Seabed Authority, 2020) highlighted the importance of sampling at the APEI sites.

Although the CCZ consists predominantly of abyssal plains, substantial environmental and biological variation is apparent (Washburn et al., 2021). This broad-scale heterogeneity is also apparent in existing data within the APEI system. In APEI-6, the shallowest of the APEIs (based on mean depth), the seabed landscape is comprised of elongated abyssal hills (Simon-Lledó et al., 2019a) with occasional seamounts over 1500 m elevation (Washburn et al., 2021). These features co-occur with other variations in the geological, chemical and biological environment (Leitner et al., 2017). At a finer scale, variations in resource supply create patches of organic enrichment that may enhance biological heterogeneity (Smith et al., 1996).

Even at the regional scale, there are relatively few studies on biology of the CCZ and the distributions of species (Taboada et al., 2018). It has been hypothesised that benthic species with widespread distributions (Drazen et al., 2021; Glover et al., 2002) exist alongside a high diversity of rare species (Smith et al., 2008; Smith, et al., 2019). Large numbers of species across all size classes in the CCZ have been documented recently, and include regional records of species or morphospecies based on imagery (Amon et al., 2017a; Amon et al., 2017b), molecular data (Janssen et al., 2015; Janssen et al., 2019), and combined molecular and morphological evidence (Dahlgren et al., 2016; Glover et al., 2016b; Gooday et al., 2020b; Wiklund et al., 2019; Wiklund et al., 2017). Records from the APEIs specifically were almost absent until recent years.

A series of recent expeditions have provided new insights into the environment of the CCZ based on a wide range of multidisciplinary data. Here, we collate these data to provide an overview of two sampled localities in the easternmost of the CCZ APEIs, APEI-6, to initiate a baseline description of the geological, physical, chemical and biological conditions on and near the seabed. Although the information presented here is far from complete, it provides a valuable insight into what is currently one of the best studied APEIs. The localities investigated in APEI-6 are then compared with sites in adjacent exploration areas to help provide an initial assessment of how representative these APEI sites are of areas potentially subject to mining pressure in the eastern CCZ. As well as having scientific interest, such information is of great importance for understanding better the environment and potential impacts of deep-sea mining on the environment to ensure effective management and regulation.

2. Methods

2.1. Study areas

Data were collected from two areas of APEI-6, the southwest (APEI-6 SW) and the northeast (APEI-6 NE; Table 1; Fig. 1; Supplementary Figure 1). In some cases, comparisons were possible to data collected in an identical way in the UK1 (United Kingdom-sponsored exploration area 1, contracted to UK Seabed Resources) contract area in the eastern CCZ (Table 1). The majority of the data used in this paper were obtained from APEI-6 SW during the RRS *James Cook* cruise 120 (JC120) expedition (Table 1) (Jones et al., 2015) and the methods described below specifically refer to this dataset, unless stated otherwise. Additional data used in this paper (Table 1) were collected during expeditions AB01 (MV1313) (Smith et al., 2013) to UK1 and AB02 (TN319) (Smith et al., 2015a) to UK1 and APEI-6 NE. A summary of the samples analysed here is presented in Table 2.

The study area in APEI-6 SW was selected based on global datasets (GEBCO, 2014) and initial multibeam data to have a similar topographical relief to that often found in contract areas (e.g. Simon-Lledó et al., 2020). The area of interest was set within a 6,300 km^2 rectangle of seafloor, approximately 20 nautical miles away from the southwestern corner of APEI-6. A much smaller area (380 km^2) was surveyed in the northeastern corner of APEI-6 during the TN319 (AB02) expedition (Table 1). Water depth within this area ranged between 3900 and 4150 m, with a similar geomorphology to APEI-6 SW. APEI-6 NE was studied opportunistically with ship time remaining at the end of cruise TN319 (AB02) during transit from the UK1 license area to the final port of San Diego.

Even the area mapped with multibeam (total of 6,680 km^2) at APEI-6 only represents a small percentage (4%) of the total area of APEI-6 (including central and buffer areas: 400 × 400 km). Undoubtedly, much of the variation found across all of APEI-6 is missed. Furthermore, some of the sample sizes in the datasets (Table 2) are small and unsuited to quantitative analysis or robust comparisons. These have been clearly indicated. Small datasets have been included as they can still provide important information for a poorly studied area like APEI-6.

2.1.1. Mapping

In APEI-6 SW, multibeam data were collected with a shipboard Simrad EM120 system on board the RRS *James Cook* (191 beams). They were processed using CARIS HIPS and SIPS software (CARIS; v8.0). The mapping data (50 m pixels) were used to delineate areas for further assessment representing characteristic landscape types: plains, ridges and troughs (Simon-Lledó et al., 2019a). A seamount, located towards

the southern end (16° 51.94′ N 122° 41.27′ W) of the study area (Fig. 1) was also assessed. Multibeam data from APEI-6 NE were collected with a shipboard Kongsberg EM302 Multibeam Sonar. Data were projected in UTM, Zone 10 N, using the World Geodetic System 1984 datum.

2.1.2. Seafloor sampling

A wide range of seabed and water column samples were obtained in APEI-6 SW (Supplementary Figure 1) following a stratified random sampling design (Simon-Lledó et al., 2019a). Although samples were stratified by topography at APEI-6 SW, we report the combined results of these samples here to represent the entire APEI-6 SW survey area. Opportunistic samples were also obtained in the northern part of UK1. For parameters that are not explored in more detail in other papers, we present data for the stratified areas and UK1 site separately in the supplementary material. Metadata for all known samples within APEI-6 and the JC120 samples from UK1 are presented in supplementary Table 1.

Sediment samples were obtained by boxcore (United States Naval Electronics Laboratory (USNEL) type, 50x50 cm square box), Megacore (Bowers & Connelly design; 10 cm internal diameter cores) and gravity core (3 m long barrel, 70 mm internal diameter core liner). Faunal samples were obtained by Agassiz trawl (3 m width, 10 mm mesh size), epibenthic sled (Brenke, 2005), baited traps (Horton et al., 2020b), and opportunistic collections from other samplers.

2.1.3. Water column sampling

Several CTD (Conductivity Temperature Depth) profiles were collected with a SBE 911plus CTD in APEI-6 SW on JC120. The UK1 site was sampled during JC120 and the ABYSSLINE cruises AB01 (MV1313, October 2013; (Smith et al., 2013)) and AB02 (TN319, February 2015; (Smith et al., 2015a)). The accuracy of the salinity and the oxygen measurements from all these cruises are expected to be within ± 0.003 g kg^{-1} and ± 0.05 mL L^{-1}, respectively. We use the TEOS-10 equation of state (McDougall et al., 2010) to derive conservative temperature (Θ, a measure of heat content) and absolute salinity (S_A: a measure of the mass fraction of salt in seawater, with units of g kg^{-1}) from the CTD measurements of conductivity, in situ temperature and pressure. Note that Θ and S_A are analogous to, but numerically different from, the more traditional potential temperature and practical salinity variables (S_P: Conductivity with temperature and pressure-dependence removed, unitless). Water samples were obtained using 10 L Niskin bottles. Samples for eDNA analysis were generally collected near seabed (5 – 10 m altitude), 50 m altitude, 100 m altitude and 500 m altitude.

2.2. Nodules

Nodules were obtained using a box corer and Megacorer at APEI-6 SW (n = 18). Nodules were removed with forceps and dried, then individually counted, measured (maximum dimension as length, and dimensions perpendicular to the maximum as width and thickness) and weighed. Densities were computed using the surface area of the box core (0.25 m^2), since nodules existed only at the sediment surface. Additional nodules were collected using the Agassiz Trawl and used for chemical analysis, but these were not individually measured.

The bulk chemical composition of the nodules was determined by inductively coupled plasma mass spectrometry (ICP-MS) on dissolved samples. Observations of microtextures and maps of the distribution of mineral phases and chemical composition were made using Scanning Electron Microscopy (SEM). More details are available in Menendez et al. (2019) and Reykhard and Shulga (2019).

2.3. Sediment properties

2.3.1. Grain size

Five Megacore deployment locations were randomly allocated with a minimum separation of 100 m within the flat, ridge and trough study areas and three locations on the deep plain during JC120 at APEI-6 SW. Additionally, one randomly allocated Megacore deployment was also obtained from the seamount at APEI-6 SW and the UK1 area during JC120. Once retrieved, cores were sliced and split into nine different sediment depths (0–0.5, 0.5–1, 1–1.5, 1.5–2, 2–3, 3–5, 5–10, 10–15, and 15–20 cm below seafloor, cmbf). Sediment grain size of each separate layer was measured independently by laser diffraction (Malvern Mastersizer; full methods in (Simon-Lledó et al., 2019a)). For subsequent analyses, mean particle size distribution for each replicate site was computed for combined 0–5, 5–10, 10–15, and 15–20 cmbf horizons.

2.3.2. Sediment pore water geochemistry

Sediments at APEI-6 SW and UK1 were obtained with a 3 m-long Gravity corer (GC) and with a Megacorer that collected the upper ~ 0.4 m of the seafloor sediments. Immediately after retrieval, the GCs were sectioned in 0.5 m intervals, oxygen concentrations measured using needle-type fiber-optical oxygen microsensors (OXR50-OI, PyroScience©) and porewater extracted with Rhizons (Rhizon CSS: length 5 cm, pore diameter 0.2 μm; Rhizosphere Research Products, Wageningen, Netherlands) inserted though pre-drilled holes in the GC liners. The same intervals were collected for each GC section, 5, 15, 25, 35 and 45 cm. Aliquots of porewater were collected for cations, nitrate and Total Alkalinity. Total Alkalinity was determined by titration against 0.0004 mol L^{-1} HCl using a mixture of methyl red and methylene blue as an indicator. Nitrate concentrations were measured with a QuAAtro nutrient analyser. For cation analyses, see Menendez et al. (2019). The porosity of the GC-sediment was calculated from the weight loss after drying the sediment at 60° C to constant weight.

2.3.3. Total carbon, nitrogen, and functionalised lipids

Total carbon (TC), organic carbon (TOC), and nitrogen (TN) were determined in surface sediments (0 – 10 mm; n = 19 for APEI-6 SW; n = 1 for seamount site in APEI-6 SW; n = 1 for UK-1). TC, TOC and TN were measured in duplicate (measurement variation <±5%) using a Carlo Erba NC 2500 CHN Elemental Analyser (full methods in (Simon-Lledó et al., 2019a)). The ratio of TOC to TN is given as the molar ratio. The total number of Megacores analysed for each area was: APEI-6 SW: Flat: 6; Ridge: 5; Trough: 5; Deep-Plain: 3; Seamount summit: 1; UK1: 1.

Total functionalised lipids of surface sediments (0–10 mm) were extracted, derivatised and quantified following the methods outlined in Jeffreys et al. (2009a). Determination and quantification of individual lipid compounds was achieved using a Trace 1300 Series gas chromatograph (splitless Triplus RHS injector; fused high temperature silica column, 60 m × 0.25 mm i.d., 0.1 μm film thickness; (5%-phenyl) methyl polysiloxane equivalent phase; DB5-HT; J&W) coupled with a

Table 1
Details of expeditions to APEI-6 and nearby comparison sites that are used in this study.

Area	Expedition	Ship	Project	Date	Central Latitude	Central Longitude	Approx. depth, m	Reference
APEI-6 Northeast	TN319 (AB02)	RV *Thomas G Thompson*	ABYSSLINE	Mar-2015	19° 30′ N	120° 10′ W	4000	Smith et al. 2015a
APEI-6 Southwest	JC120	RRS *James Cook*	MIDAS	Apr-2015	17° 00′ N	123° 00′ W	4200	Jones 2015
UK1 North	JC120	RRS *James Cook*	MIDAS	Apr-2015	13° 28′ N	116° 36′ W	4100	Jones 2015
UK1 Stratum A	MV1313 (AB01)	RV *Melville*	ABYSSLINE	Oct-2013	13° 49′ N	116° 36′ W	4100	Smith et al. 2013
UK1 Stratum B	TN319 (AB02)	RV *Thomas G Thompson*	ABYSSLINE	Mar-2015	12° 29′ N	116° 36′ W	4200	Smith et al. 2015a

Thermoquest Scientific ISQ-LT mass spectrometer, see Jeffreys et al. (2009a). Concentrations of individual compounds were determined by comparison of their peak areas with those of the internal standards and were corrected after calculation of their relative response factors (Kiriakoulakis et al., 2004).

2.3.4. Environmental DNA and metabarcoding

Sediment was aseptically sampled from Megacores at the SW site. The following sediment depth layers were used for analysis of eDNA studies: 0–1, 1–2, 5–6, 10–12 and 22–24 cmbf. Genomic DNA was extracted from sediment samples using the FastDNA Spin Kit for Soil (MP Biomedicals, USA) following the manufacturer's protocol. Additional extraction blanks containing only the FastDNA Spin Kit reagents were processed with the sediment samples. The concentrations of DNA from all samples was below 0.1 ng mL^{-1} and required further concentration. DNA was concentrated using Zymo Clean & Concentrator-5 kits with a 2:1 DNA Binding Buffer ratio and eluted into 50 mL sterile, DNase-free water. The V4 region of the 16S bacterial and archaeal rRNA gene was amplified by the polymerase chain reaction (PCR) using the oligonucleotide primers Pro515f/Pro805r. These also contain Illumina adapter sequences and sample-specific barcode sequences (Caporaso et al., 2012; Caporaso et al., 2011). The amplified 16S rRNA gene products and extraction blanks were sequenced using an Illumina MiSeq at the National Oceanography Centre, Southampton. Illumina paired-end 16S rRNA reads were joined and analysed with QIIME (Quantitative Insights Into Microbial Ecology) microbiome analysis package, version 2–2017.9 (Caporaso et al., 2010). The DADA2 pipeline within QIIME 2 was implemented for sequence quality control and chimera removal. Operational Taxonomic Units (OTUs) that were observed in the PCR blanks were considered to be contaminants and were filtered from the samples. Taxonomy was assigned using the Silva 132 database (Quast et al., 2012). Taxa or OTUs were defined at 99% 16S rRNA gene identity.

2.4. Faunal samples

Macrofaunal samples were processed using live-sorting cold-chain protocol for DNA taxonomy (Glover et al., 2016a), which included at-sea abundance counts, morphological study and imaging. Sediments (0–150 mm depth) were sieved at 300 µm and sorted cold under a dissecting microscope. During collection, topwater was lost from several boxcores in the southwestern site (but not in the northeastern site) and hence abundance data should be considered non-quantitative. Scavengers were sampled by means of a baited trap (Horton et al., 2020b) deployed for < 40 h at two stations (JC120-008 and JC120-039; baited with tuna) at APEI-6 SW and a second trap type (Leitner et al., 2017) at one station (AB02-TR13; baited with one mackerel) at APEI-6 NE.

Molecular methods and primers for markers 18S, 28S, 16S and mitochondrial cytochrome oxidase subunit 1 (CO1) follow recommended protocols (Glover et al., 2016a). For this study, conspecificity was confirmed at the molecular level using sequence alignment. Studies in preparation, and already published, will include full phylogenetic analyses of groups in question (e.g. Wiklund et al., 2017). Data for individual samples, identifications, materials, DNA vouchers and types are reported in ongoing taxonomic publications (Dahlgren et al., 2016; Glover et al., 2016b; Wiklund et al., 2017). We do not report here studies of Crustacea, but include all other metazoan taxa, for which sequences were available. Data from within the study areas (APEI-6 and UK1) from JC120, AB01 and AB02 were used to compare the APEI-6 region with the exploration contract sites.

2.4.1. Autonomous seabed photography

Vertically-facing seabed photographs were collected in APEI-6 SW using the autonomous underwater vehicle (AUV) Autosub6000 (camera: Grasshopper2, lens focal length: 12 mm, frame resolution: 2448 × 2048 pixels; photograph interval 850 ms) travelling (speed 1.2 ms^{-1}) along zig-zag image transects with random start points. The image data were post-processed as described in Simon-Lledo *et al.* (2019a). The full resultant dataset was composed of data from 88,630 non-overlapping

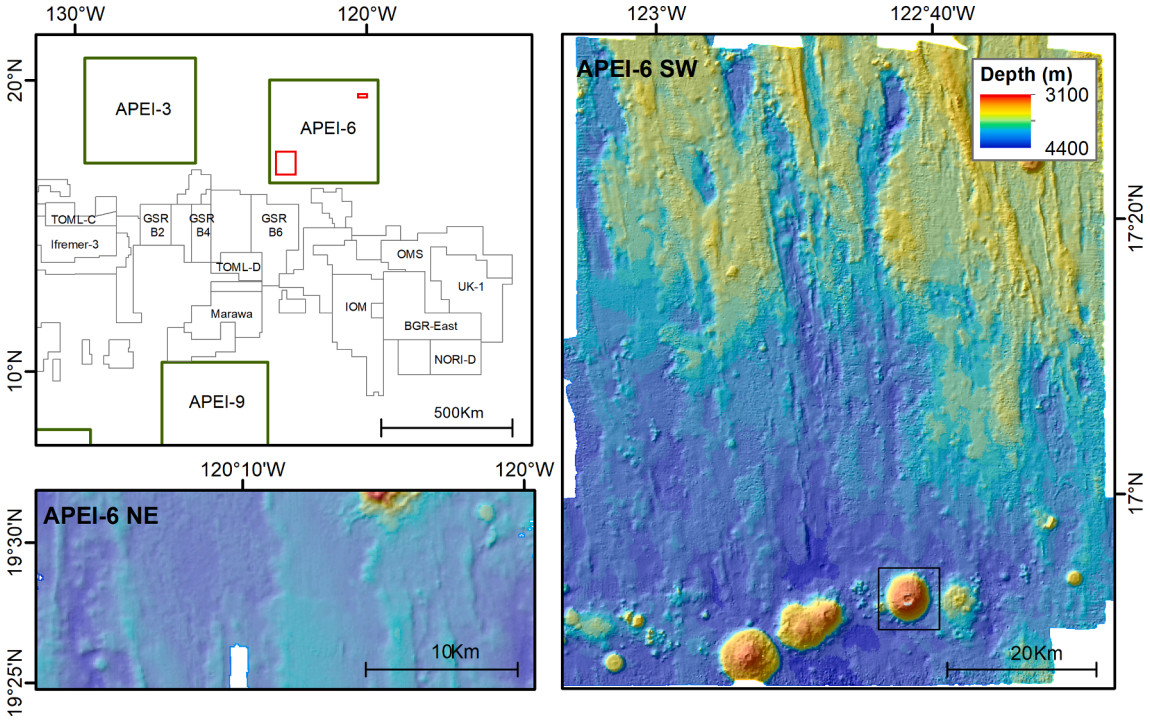

Fig. 1. Map of APEI-6 showing shipboard multibeam bathymetry for southwestern area (right) and northeastern area (lower left). Seamount investigated indicated by black box on right figure. Top left map shows position of APEI-6 relative to nodule exploration contract areas (labelled by contractor) and nearest APEIs. The extent of the SW and NE areas are indicated as red rectangles.

images collected at altitudes of 2–4 m, representing a seafloor area of 160,500 m^2. A subset of 12 randomly-selected transects were used for quantitative biological analysis (10,052 images, covering a seabed area of 18,582 m^2).

A total of 2571 images were obtained on one dive at APEI-6 NE using the AUV REMUS6000. The vehicle travelled at 1.5 ms^{-1} while taking photographs every 3.5 s at varying altitudes (<11 m, mean altitude: 8.5 m). The AUV was equipped with a Prosilica GT3400 colour camera (3384 × 2704 pixels). Images were scaled using parallel green lasers (200 mm apart; Micro Sea laser). The dataset covered an approximate area of 40,800 m^2 of seabed, but given the lower resolution and higher altitude of collection of these images, these were only used to detect large [>5 cm] megafauna.

2.4.2. Towed-camera photography

The UK National Oceanography Centre towed camera platform HyBIS was used to carry out video and photographic transects in more topographically complex areas, such as the seamount investigated in APEI-6 SW. HyBIS was equipped with two video camera systems (including parallel red lasers attached 110 mm apart for scaling). Video was recorded using a forward-facing Bowtech L3C-550C video camera and a vertically-mounted *Insite Pacific Super-Scorpio* video camera. The *Super-Scorpio* camera (lens focal length: 26.3 mm in air) was also used to take stills at 4 s intervals (frame resolution 4672 × 2628 pixels). A total of 3106 frames were collected at the seamount. Each picture was classified as imaging either exposed bedrock stratum (e.g. where pillow lavas were visible), or sediment.

For subsequent quantitative analysis, frames taken too high (no red laser dots visible) or too low (taken before and after seafloor collisions) above the seafloor were removed. Overlap between pictures was also manually removed by visualisation of consecutive remaining pictures. This left 350 pictures for quantitative analysis, covering a total area of 5,191 m^2. On average, these were collected at a higher altitude above seabed (mean altitude = 4.3 m, mode = 6.20 m) than at the other sites imaged by AUV (mean altitude = 3.10 m, mode = 2.91 m) within APEI-6 SW. Thus, smaller sized animals could be potentially underestimated at the seamount, relative to the other locations. Because of the relatively small sample size at the seamount, only ecological measures that are less sensitive to small sample sizes were used (e.g. numerical density of fauna (Simon-Lledó et al., 2019a)).

2.4.3. Baited camera video

Fish and scavenger communities were sampled at APEI-6 NE with a baited camera system described in detail in Leitner et al. (2017). In brief, the system is a free-falling stereo-video lander system. The HD camera pair was geometrically-calibrated, and mounted horizontally at a slightly oblique downward angle such that they provided a 1.86 m^2 half-elliptical field of view. The lander was baited with ~ 1 kg of Pacific mackerel (*Scomber japonicus*), which was maintained in the centre of the field of view 1 m in front of the cameras. Video was recorded in 2-minute intervals with 8-minute rest periods to extend battery life to 24-hours and to minimize light disturbance to bait-attending fauna.

2.4.4. Automatic detection of nodules in images

Nodule cover (%) was quantified from the AUV imagery collected at APEI-6 SW using the Compact-Morphology-based polymetallic Nodule Delineation method (CoMoNoD; (Schoening et al., 2017)). The CoMoNoD algorithm calculates the size of each nodule (i.e., seafloor exposed area) detected in an image, enabling the calculation of descriptive nodule statistics. Note that it is currently not possible to relate directly the image-based assessments of seabed nodule cover with those made by direct sampling methods (Gazis et al., 2018; Schoening et al., 2017). Only visible nodules ranging from 0.5 to 60 cm^2 (i.e. with maximum diameters of ~1 to ~10 cm) were considered for analysis to avoid inclusion of large non-nodule formations. Average nodule densities were calculated on an image basis, whereas average nodule sizes were calculated on an individual nodule basis.

Table 2
Summary of sample numbers used for analysis at APEI-6 and at UK-1 (on cruise JC120 only). Note some additional samples are available (See supplement S1). NA = Not Available.

Parameter	Method	Sample Unit	APEI-6 NE Samples	APEI- 6 SW Samples (not seamount)	APEI-6 SW Seamount Samples	UK-1 Samples (JC120)	Notes
Water temperature, salinity and oxygen	Water sampling rosette and sensors	Regular (24 Hz) sensor-based measurements	1	6	1	1	Previously unpublished
Nodule density, dimensions and weight	Box core	One core (0.25 m^2)	2	18	NA	1	Previously unpublished
Seabed nodule coverage	Photography (automated processing)	Photographs (~1.7 m^2)	0	197,900	NA	0	See Simon-Lledo et al., 2019b
Grain size, sediment biogeochemistry	Megacore	One core (0.0079 m^2)	0	19	1	1	See Simon-Lledo et al., 2019a for grain size; Biogeochemistry results previously unpublished
Sediment metals	Megacore	One core (0.0079 m^2)	0	4	0	1	See Menendez et al., 2019
Sediment oxygen penetration	Gravity core	One core	0	5	0	1	Previously unpublished
Macrofaunal species richness	Box core	Total of all box cores	NA	15	NA	1	Previously unpublished
Benthic megafauna and trace properties	Photography (manual annotation)	Photographic transect (1320 m^2)	NA	12	NA	0	See Simon-Lledo et al., 2019a
Qualitative megafauna and habitat description	Photography (manual assessment)	Total area (m^2)	21853.5	NA	5191	NA	Previously unpublished
Microbes	Megacore	Subsamples from one core	NA	96	NA	6	JC120 results previously unpublished. Additional material from APEI-6 NE in Wear et al. (2021) and Lindh et al. (2017)

2.5. Detection and classification of megafauna in images

Megafauna specimens (>10 mm) in selected quantitative imagery were identified up to the lowest taxonomic level possible and measured using either BIIGLE software (Bielefeld Image Graphical Labeller and Explorer; (Langenkämper et al., 2017)) for the APEI-6 SW images, or Image J (Schneider et al., 2012) for the APEI-6 NE dataset. Several revisions were performed to ensure consistency of fauna morphotype identifications with a megafauna catalogue developed upon international taxonomic expert consultations (Simon-Lledó et al., 2020), providing a standardised megafauna morphotype (mtp) code. Megafauna are assigned a standardised open nomenclature (Horton et al., 2021). Quantitative seabed megafauna data collected at the UK1 AB01 area (Amon et al., 2016) was reassessed and aligned in accordance with this standardized catalogue to enable direct comparisons between different areas. In addition, large (>5 cm) megafauna visible in images collected at the APEI-6 NE area were also identified but not quantified. Invertebrates living in a shell or tube (e.g. most polychaete and gastropod taxa) were excluded from analyses. Paleo-geological features observed on the seafloor were annotated and measured, including: whale bones and shark teeth, *Paleodictyon nodosum* facies, and any non-polymetallic nodule (angular shaped) geologic formations, from cobbles to large rocks. Identifications were improved by referencing to collected specimens.

3. Results and discussion

3.1. Oceanography

The deepest water masses of the CCZ consist of Lower Circumpolar Water (LCPW) and North Pacific Deep Water (NPDW) (Johnson and Toole, 1993). CTD profiles at APEI-6 indicate the presence of low-salinity (34.86 S_A) and low-oxygen (2.65 mL L^{-1}) NPDW around 3600 m ($\Theta > 1.30$ °C), but also the eastward penetration of saline and more oxygen-rich LCPW below the NPDW layer extending as far as UK1 (117°W). The presence of LCPW this far east in the tropical Pacific is unexpected. LCPW enters the CCZ from the west, south of the Hawaiian Ridge around 160°W, before travelling north-northeastwards (Juan et al., 2018). LCPW is formed of North Atlantic Deep Water (NADW) and Antarctic Bottom Water (AABW), which originate from the North Atlantic and the Weddell Sea, respectively (Wijffels et al., 1996). The LCPW is the coldest ($\Theta < 1.2$ °C) densest water mass with high salinity and high oxygen levels owing to its relatively recent ventilation. In contrast, NPDW is the oldest low-oxygen water mass formed internally without surface sources from the upwelled LCPW in the North Pacific (Kawabe and Fujio, 2010). In the CCZ, this water mass is somewhat warmer ($1.2 < \Theta < 2$ °C) than the LCPW and flows southward in the eastern CCZ, along the western flank of the East Pacific Rise, which is to the east of APEI-6.

Breaks in the slopes of the S_A/Θ and O_2/Θ curves between APEI-6 SW and the UK1 study area (Fig. 2: a and b) indicate differences in the deep-water mass separation, which occurs on a colder isotherm at APEI-6 ($\Theta = 1.23$ °C) than at UK1 ($\Theta = 1.30$ °C). This observation is consistent with an expected decrease in the volume of northward flowing LCPW between UK1 and APEI-6. It is not known if the changes in water masses observed are sufficient to lead to other environmental effects, as they are elsewhere (Puerta et al., 2020; Reinthaler et al., 2013).

Current speed data are very limited in APEI-6. A single 24-hour deployment (Leitner et al., 2017) at APEI-6 NE recorded very low average (0.03 m s^{-1}) and maximum (0.23 m s^{-1}) bottom current speeds. Currents of the bottom 50–100 m in the CCZ are typically below 0.05 m s^{-1} when averaged over several months (Hayes, 1979). However, mesoscale features affect deep velocities and events with amplitudes > 0.1 m s^{-1} can last several weeks (Kontar et al., 1994). Peak velocities of up to 0.25 m s^{-1} have been registered (Aleynik et al., 2017; Amos and Roels, 1977). Deep low-frequency currents intensify in the bottom boundary layer within ~ 100–30 m from the seabed in this region and veer counter-clockwise toward the bottom consistent with an Ekman layer dynamic (Hayes, 1980; Kontar and Sokov, 1994). In addition, higher-frequency internal inertia-gravity waves, including semidiurnal tides and near-inertial waves, are generated by barotropic tides, eddies and mean currents flowing over rough topography, which includes seamounts, ridges, and troughs present in the APEI-6 area. These internal waves and the associated turbulence may act to amplify the dispersion of potential mining-related plumes (Aleynik et al., 2017).

3.2. Seabed morphology

The area surveyed for this study covers approx. 6,300 km^2 in APEI-6 SW and 380 km^2 APEI-6 NE, representing around 4.1% of APEI-6 (Fig. 1). Water depths at APEI-6 SW range from 3400 m on the tallest seamount down to 4400 m in the deepest parts surveyed. APEI-6 SW

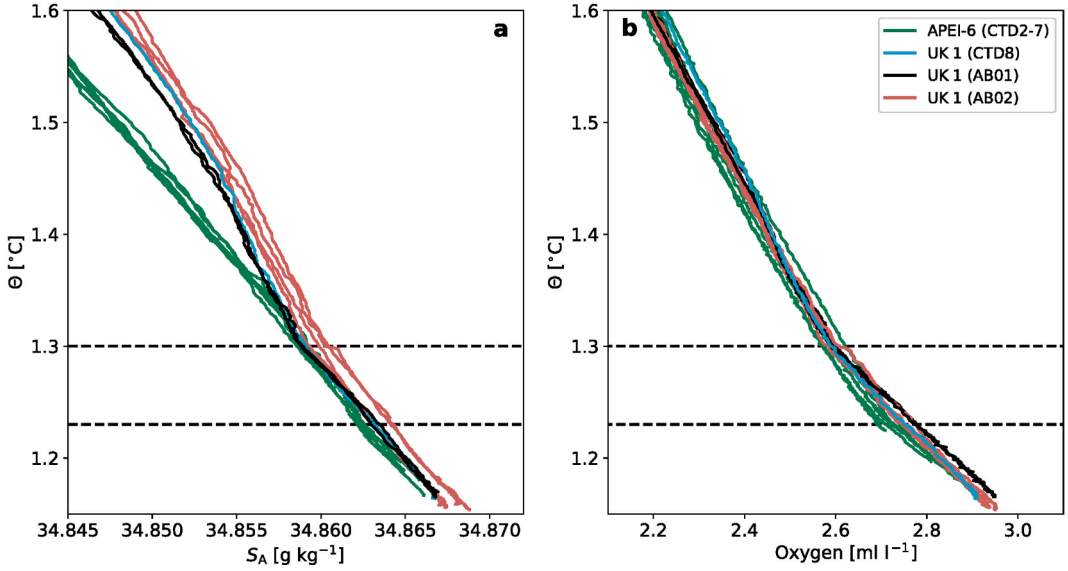

Fig. 2. (a) Absolute Salinity S_A and (b) dissolved oxygen concentration versus Conservative Temperature Θ for the CTD profiles taken in APEI-6 SW and UK1 regions. Note that Conservative Temperature and Absolute Salinity are not the same as in situ temperature and practical salinity, as measured by the CTD.

contains an E-W orientated chain of seamounts/knolls (see seamount section for more detail) in the southern half, and a sequence of ridges, flatter areas and troughs (horst-and-graben structure) in the northern half of the study area, with a few seamounts/knolls scattered in between these two areas. The horst-and-graben morphology has a NNW-SSE orientation and covers depths between 3850 m and 4350 m. Troughs are on average spaced ca. 15 km apart. This morphology appears characteristic of the remainder of APEI-6 (Washburn et al., 2021) and the CCZ in general (Haxby and Weissel, 1986; Juan et al., 2018; Rühlemann et al., 2011; Winterer and Sandwell, 1987). The rugose topography of the CCZ is caused by tectonic processes connected to the formation of the East Pacific Rise, which lies to the east (Wessel et al., 2006) and low sedimentation rates have limited homogenisation of the topography by sediment blanketing (Juan et al., 2018). At APEI-6, sub-bottom profiles indicate up to three acoustic units of sediment, with the uppermost (AU3) likely comprised of unconsolidated sediments up to 18 m thick, a deeper distinct layer (AU2) of older (possibly Miocene) consolidated sediments and in some places a third high-amplitude unit (AU1), likely

Table 3
Average and 95% confidence intervals for parameters measured across APEI-6 and other relevant areas. Contract areas: German Federal Institute for Geosciences and Natural Resources (BGR) eastern contract area; UK1: UK Seabed Resources Limited eastern contract area; L'Institut Français de Recherche pour l'Exploitation de la Mer (IFREMER); InterOcean Metals contract area (IOM). For nodule dimensions n: number of nodules measured, l = length, w = width, h = height.

Parameter	APEI-6 SW	APEI-6 NE	APEI-6 Seamount	Contract areas	Reference for contract area values
Average depth, m	4200	4000	3500	4110: UK1 4840: BGR W1 4240: BGR E1	This study Rühlemann et al. 2011
Area size, km^2	6,300	380	36	60,000: UK1 17,000: BGR W1 58,000: BGR E1	Rühlemann et al. 2011
Seabed Temperature (in situ), °C	1.54		1.55	1.51: UK1	this study
Seabed Conservative Temperature, Θ	1.20		1.29	1.17: UK1	this study
Seabed salinity (practical salinity)	34.68		34.68	34.69: UK1	this study
Seabed Absolute Salinity (S_A, g kg^{-1})	34.86		34.86	34.87: UK1	this study
Seabed Oxygen, mL L^{-1}	2.80		2.61	2.91: UK1	this study
Nodule density, no m^{-2}	314 (212–423)			16: UK1	this study
Nodule dimensions, mm	n = 1417 nodules; l = 19.8 (19.4–20.3) w = 15.5 (15.1–15.8) h = 9.2 (9.0–9.4)			n = 1260 : UK1 l = 39 ± 8 : UK1 l = 40–80: BGR E1 l = 40–75: IFREMER E	Smith et al. 2013; Rühlemann et al. 2011; Veillette et al., 2007a,b
Nodule weight, kg m^{-2}	1.33 (0.81–1.9)			1.7: UK1 (1 box core) 1.7–57: UK1; 8.0: BGR W1; 13.7: BGR E1	this study Rühlemann et al. 2011
Seabed nodule coverage (%)	6.6 (SD 4.9) range = 0–48				
Grain size, μm (sample means, min - max)	0 to 5 cm: 6.53–9.21 5 to 10 cm: 6.19–11.16 10 to 15 cm: 5.72–20.08 15 to 20 cm: 5.68–20.15		0 to 5 cm: 27.62 5 to 10 cm: 21.72 10 to 15 cm: 15.97 15 to 20 cm: 17.43	UK1: 0 to 5 cm: 18.06 5 to 10 cm: 17.6 10 to 15 cm: 17.58 15 to 20 cm: 18.74	this study
Total Organic Carbon (TOC, %)	0.43 ± 0.03		0.22	0.71: UK1 0.62: BGR 0.52: GSR 0.24: APEI-3	this study Volz et al., 2018
Total Nitrogen (TN, %)	0.01 ± 0.004		0.06	0.14: UK1	this study
molar TOC:TN ratio	4.62 ± 0.14		4.50	5.7: UK1	this study
$CaCO_3$, %	0.4 ± 0.09		73.3	0.1: UK1	this study
Sediment oxygen penetration depth, m	>2			1: UK1 1: GSR 3: IOM	this study Volz et al., 2018
Fe (wt %)	6.75 ± 1.29			6.06 ± 0.105: UK1	this study
Mn (wt %)	27.4 ± 2.12			28.2 ± 3.01: UK1	this study
Mn:Fe	4.06			4.65: UK1	this study
Cu (ppm)	9770 ± 2150			7980 ± 640: UK1	this study
Ni (ppm)	12700 ± 1630			10600 ± 1130: UK1	this study
Co (ppm)	2500 ± 666			1220 ± 90.1: UK1	this study
ΔREY (ppm)	1000 ± 340			813 ± 38.4: UK1	this study
Al (wt %)	2.31 ± 0.238			2.04 ± 0.165: UK1	this study
P (wt %)	0.12 ± 0.01			0.13 ± 0.01: UK1	this study
Li (ppm)	103 ± 25.2			173 ± 4.32: UK1	this study
Macrofaunal species richness	25				this study
Megafaunal xenophyophore density, ind. m^{-2}	2.55 (1.74–3.32)	NA	0.19	0.65 (0.51 – 0.78): UK1	Amon et al 2016
Megafaunal metazoan density, ind. m^{-2}	0.38 (0.28 – 0.46)	NA	0.07	1.08 (0.76–1.25): UK1 0.44: TOML-D	Amon et al. 2016; Simon-Lledó et al. 2020
Megafaunal metazoan taxon richness, total morphospecies	123 (in 18,852 m^2 of seabed)	34 (in 850 m^2)	37 (in 5120 m^2 of seabed)	110 (in 4204 m^2 of seabed): UK1 189 (in 20200 m^2 of seabed): TOML-D	Amon et al. 2016; Simon-Lledó et al. 2020
Paleodictyon density, trace m^{-2}	0.33		0		Durden et al. 2017

bedrock, which outcrops in places (Alevizos et al., submitted).

3.3. Nodules

The shape (sub-spherical with smooth surfaces) and size (mean maximum diameter ~ 20 mm) of nodules recovered across APEI-6 SW were smoother and smaller than those measured at UK1 (mean maximum diameter 39 mm from ABYSSLINE surveys), IFREMER (Veillette et al., 2007b), E1 BGR (Rühlemann et al., 2010) and the eastern CCZ (IOM, (International Seabed Authority, 2010); Table 1). Caution should be taken in making direct comparisons as nodule size distributions are variable even across fine scales (tens of metres) and publicly-available nodule size distribution data are limited.

Nodule density (mean 200 – 632 m^{-2}), size (maximum dimension 16.1 – 21.9 mm), and estimated resource by mass (0.55–2.56 kg m^{-2}) varied at the landscape scale across APEI-6 SW (Table S2). Average nodule coverage calculated from seabed photographs at the APEI-6 SW was 6.6 % (Table 3), again with high spatial variation (Table S2; Fig. 3: c-d). These variations are consistent with local variations observed across morphologically different seafloor areas within the BGR license area in the eastern CCZ (Mewes et al., 2014; Peukert et al., 2018; Rühlemann et al., 2011), where nodule resource (0.2–30 kg m^{-2}) and size (10–120 mm) varied at a similar spatial scale of tens to hundreds of metres. Regional scale investigations suggest nodule abundances are

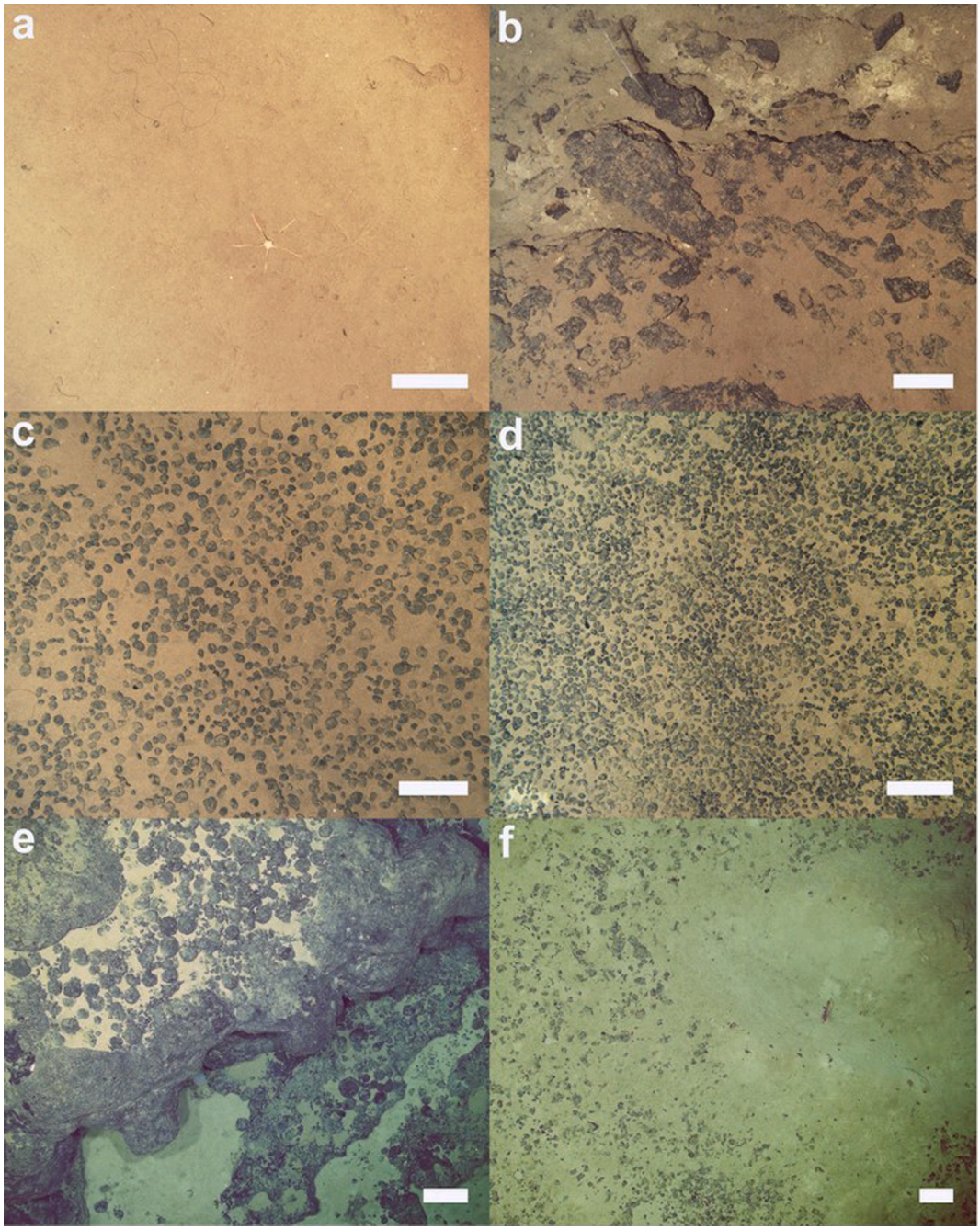

Fig. 3. Representative images of seafloor in different areas of APEI-6-SW. a to d: collected using Autosub6000. e to f: collected using HyBIS towed camera. a) Nodule-free seabed. b) Exposed bedrock, boulders, and cobble seabed. c) Densely nodule-covered seabed (35% coverage). d) Densely nodule-covered seabed (47% coverage). e) Fe-Mn crust coated pillow basalt and cobble seabed at the western flank of the seamount crater. f) Fine sediment and talus fragments seabed at the centre of the seamount crater. Scale-bars represent 25 cm.

higher in the central CCZ than at the periphery, where most of the APEIs are located (McQuaid et al., 2020). In general, the mass per unit area of the nodules is controlled more by the size of the nodules rather than their numerical density (Rühlemann et al., 2011). This variation in nodules is typically attributed to variations in sedimentation, including those related to topography (Juan et al., 2018; Mewes et al., 2014; Rühlemann et al., 2011).

3.3.1. Nodule composition

The nodules consist of alternating concentric layers of Mn-rich oxides (birnessite) and Mn-Fe-rich oxyhydroxides (vernadite); small quantities of aluminosilicate-rich detrital material and minor quantities of fluorapatite occur in pore spaces (expanded in Menendez et al 2019). Phillipsite, a marker of volcanic activity, was present in the nodules assessed from APEI-6 SW but not UK-1 (expanded in Reykhard and Shulga, 2019). Compared to nodules from the UK1 contract area, and other parts of the CCZ, APEI-6 SW nodules have on average slightly higher concentrations of Fe (6.75 wt%), Co (2500 ppm) and total rare-earth elements (1000 ppm), and lower concentrations of Mn (27.4 wt %) and Li (103 ppm) (Table 1). There is little variation in the chemical composition of nodules within APEI-6 (expanded in Menendez et al., 2019). Together with the small size of the nodules, their chemical composition indicates that the APEI-6 nodules acquire a greater part of their metals from a hydrogenous source (seawater) relative to a diagenetic source (sediment pore waters) compared to other parts of the CCZ assessed to date (Bau et al., 2014; Hein et al., 2013; Menendez et al., 2019; Reykhard and Shulga, 2019).

3.4. Sediment properties

The visual appearance of the seafloor (Fig. 3) showed soft sediments, nodules and regular features associated with bioturbation (mounds, trails and faecal deposits). Larger pits in the sediment of probable biogenic origin (expanded in Marsh et al., 2018) were seen in side-scan sonar data. These are hypothesised to result from the feeding activities of beaked whales and also occur in UK1 (Marsh et al., 2018), on seamount summits in APEI-4 and 7 (Leitner et al., submitted) as well as other areas in the Pacific (Purser et al., 2019). Occasional rock outcrops were observed (Fig. 3: b,e; (Alevizos et al., submitted)).

Radiolarian-bearing pelagic sediments were common across APEI-6 SW. These fine-grained muds are consistent with other seabed sediments across the wider CCZ (Mewes et al., 2014). Surface sediments (0–5 cm) at APEI-6 SW were dominated by clay to fine silt particles < 7.8 μm (58–68 % of dry weight), and medium to very coarse silt grains 7.8–63 μm (28–39 %). As found elsewhere, clays at APEI-6 SW were in most cases poorly crystallized smectite, sometimes also illite and quartz; feldspar and chlorite occur less frequently (Riech and von Grafenstein, 1987). Deeper sediments (5–20 cm) at the deep plain and flat followed this same pattern, whereas replicate cores at the ridge and trough sites were more heterogeneous, with median values ranging from 5.9 to 31.8 μm (see Table S4). Similar granulometries (~70% particles < 6.3 μm) were found on surface sediments at the E1 BGR contract area (Mewes et al., 2014), slightly finer grain sizes (median: 2–4 μm) were reported within APEI-4 (western CCZ) and within the SE IFREMER contract area (Halbach et al., 1979; Renaud-Mornant and Gourbault, 1990), whereas within the UK1 contract area the median grain size was much coarser, and described a bimodal size distribution pattern increasing with depth (see Table S4).

In APEI-6 SW the gravity cores (Fig. 4) consisted of a fine mud, consistently of reddish brown colour with no notable layers although there were occasional white inclusions at various depths within the cores. Nodules were usually only found on the surface of the cores. On very few occasions were nodules found deeper (e.g. at 17 cm depth in a gravity core (JC120-GC2) at the trough site; Fig. 4) but no Mn-nodules or Mn-nodule fractions were found in the deeper parts of the sediments. These characteristics were also shared with the single gravity core

Fig. 4. Photographs of sectioned gravity cores from APEI-6 (GC01-05) and UK1. The image is cropped to the length of the shortest core (GC06). For scale, the width of each core is 70 mm.

obtained at UK1 (on JC120). Buried nodules have been found more commonly in other samples elsewhere in the CCZ (Mewes et al., 2014) including from other samples at UK1 (Smith et al., 2013). Usually, sediments in the CCZ have 2–3 lithostratigraphic units of variable thickness comprising sediments from Late Eocene to Quaternary age (Riech and von Grafenstein, 1987) and mainly consist of radiolarian and diatom-bearing silty clay (Mewes et al., 2014). No information on sedimentation rates at APEI-6 is available.

The porosity of the sediment was similar in the different APEI-6

cores, with only little downward compaction (decreasing from ~ 0.9 ϕ [ratio of volume of void space to total volume of material] close to the sediment surface to ~ 0.8 ϕ at 3 m). In the UK1 contract area the porosity was slightly higher at the sediment surface (~0.95 ϕ) and changed even less with depth (~0.85 ϕ at 2 m). The UK1 information is only based on one core, which may not be representative of the whole site.

3.5. Sediment geochemistry

Porewater nitrate concentrations were around 50 μmol L^{-1} and stayed constant throughout the core in both APEI-6 SW and UK1. The nitrate profiles are similar to other CCZ studies (Jeong et al., 1994; Mewes et al., 2014) and suggest that organic matter degradation is largely driven by oxic respiration. Low levels of organic carbon degradation are also confirmed by the Total Alkalinity concentrations, close to seawater at all sites (2.2 to 2.4 mmol L^{-1}). The major cations in the porewater have seawater concentrations. In the upper 3 m of the sediment, concentrations of metals, in particular Fe and Mn, were very low (<1 μmol L^{-1}), consistent with the oxic conditions in the sediments (Menendez et al., 2019).

For most major elements, there was little down-core variation in the solid phase of the sediments and concentrations were similar in the samples from APEI-6 SW and UK1 (expanded in Menendez et al., 2019). For example, manganese content was about 0.5 wt% and Fe about 7 wt% at APEI-6 SW, similar to other CCZ sediments (Mewes et al., 2014). This indicates that the environmental factors shaping the element distribution were similar in the different areas; i.e., sedimentation happened under quite constant conditions and the detrital component building up the sediments had a similar composition. Correlations of the redox active element Fe with, for example, Ca, showed that the Fe is likely controlled by water column productivity/input and not by diagenetic mobilization in the sediment.

The oxygen penetration depth (OPD) was similar in the different geomorphological settings of APEI-6 SW, with oxygen still detected at>2.0 m sediment depth (expanded in Menendez et al., 2019). Oxygen penetration was shallower at UK1, with oxygen only detected in the upper 1.5 m. OPDs are of the same order of magnitude as previously measured in the CCZ (1.8–3 m, (Mewes et al., 2014): 1–4.5 m (Volz et al., 2018)). However, we found in the UK1 area that sites with shallower OPD are characterized by bigger nodules.

3.6. Sediment biogeochemistry

3.6.1. Total carbon, organic carbon and nitrogen distributions

TOC, TN, TOC:TN and $CaCO_3$ (Table 3) were similar at all areas of APEI-6 assessed (Table S5) and similar to those measured elsewhere in the CCZ (Khripounoff et al., 2006; Volz et al., 2018). However, the single sample taken at UK1 had a greater abundance of TOC and TN than the other sites. Molar TOC:TN at APEI-6 SW were just below 5, which is similar to marine phytoplankton and undegraded phytodetritus sources of organic compounds (C/N ratios of 5–7) (Santos et al., 1994). These values are similar to those reported previously in the CCZ (Khripounoff et al., 2006; Müller, 1977). TOC content in nodules from APEI-6 SW and UK-1 area (0.13–0.17 %) is lower than in sediments (expanded in Shulga, 2017, 2018).

3.6.2. Molecular composition of organic matter in surficial sediments

Sedimentary distributions of lipid biomarkers (Table S5) in the samples were complex and total quantifiable concentrations varied between sites at APEI-6 SW (average 3947 ng g^{-1} ± 1078 95% C.I.) but are comparable with a single sample from UK1 (5225 ng g^{-1}). Total lipid concentrations are lower at APEI-6 SW than previously reported for the Equatorial Pacific (Wakeham et al., 1997) but comparable with Atlantic abyssal plains (Neto et al., 2006; Santos et al., 1994). There are no significant differences between major compound classes and sites at APEI-6 SW (Table S5). A wide variety of compounds were identified at APEI-6 SW (111 in total) from both marine and terrestrial sources. However, sedimentary organic material was predominantly marine in origin, as indicated by TOC:TN ratios, (see above) and lipid biomarkers, e.g., the C_{16}/C_{26} fatty acid ratio, an indicator of the relative contribution of marine (C_{16}) vs. terrestrial (C_{26}) organic matter (Meyers et al., 1984), which ranged from 2 to 20 (mean = 6.3 ± 4.6 S.D.).

3.6.3. Sources and quality of organic matter

Phytodetritus is an important food source for deep-sea organisms at APEI-6 SW. Components of this material include dietary fatty acids that are required for reproduction, growth, cell membrane structure and function, energy storage and hormone regulation (Neto et al., 2006). Lipid profiles at APEI-6 SW showed characteristics of phytodetrital input, including short chain saturated fatty acids ($<C_{20}$), mono- and poly-unsaturated fatty acids (MUFAs and PUFAs respectively), in addition to certain C_{28} and C_{29} sterols, mid-chain diols and alkenones (Conte et al., 2003; Rampen et al., 2010; Wakeham et al., 2002).

Microalgal contributions to sedimentary organic matter at APEI-6 SW were evident from fatty acid distributions, which were dominated by C_{16}, C_{18} saturated and monounsaturated homologues at APEI-6 SW. The ratio of C_{18}:C_{16} fatty acids has been used to assess the relative input of dinoflagellates and prymnesiophytes to diatoms (Reuss and Poulsen, 2002). Concentrations of PUFAs were highly variable but formed an appreciable contribution to the sediments ranging from 0.8 to 15.6% of the total quantifiable lipids. This indicates that the sedimentary organic matter was relatively well degraded. The Unsaturated:Saturated fatty acid ratio at APEI-6 SW was ~ 0.6, further indicating well degraded OM. Eicosapentaenoic acid, $C_{20:5(n-3)}$ and docosahexaenoic acid, $C_{22:6(n-3)}$ are essential PUFAs, being diagnostic biomarkers for phytoplankton, and were present at all APEI-6 SW sites, but in minor quantities representing < 5% of the PUFA pool.

Sterols are more refractory than fatty acids and provide further indications of the provenance of organic matter. The C_{27}:C_{29} sterol ratio can be used to assess invertebrate / phytoplankton contributions; this ratio was ~ 0.4 at APEI-6 SW, suggesting a greater input of phytosterols to the sediments. The dominant sterol at all sites was $C_{29}\Delta^5$ accounting for ~ 55% of the sterol pool across APEI-6 SW, and is one of the most common sterols of diatoms (Rampen et al., 2010). Long chain alkenones, biomarkers for coccolithophores e.g. C_{37} alkadien-2-one, were present in minor amounts (<2% total lipids) across APEI-6 SW. The nature of organic matter at the seafloor is, for example, thought to affect the ecology of the common deposit feeding organisms that use this as their food source (Wigham et al., 2003).

3.6.4. Planktonic contributions to organic matter

Concentrations of lipids in surficial sediments in APEI-6 SW were lower than those reported for surficial sediments in the Equatorial Pacific and an order of magnitude lower than particulate organic matter in the water column in the Equatorial Pacific (Wakeham et al., 1997). Biomarkers attributed to herbivorous mesozooplankton e.g. $C_{20:1}$ and $C_{22:1}$ fatty acids were present in sediments from all sites accounting for between 2% and 16% of the fatty acid pool. Cholesterol ($C_{27}\Delta^5$) accounted for ~ 20% of the sterols in the sediments of APEI-6 SW. Cholesterol is synthesised by phytoplankton and is also a major constituent of invertebrate (e.g. zooplankton) lipids and may also be indicative of faecal pellets contributing to the organic matter (Wakeham et al., 2002). Lipids play important roles in many biological processes and they are useful tracers of organic matter sources and alteration both in sinking particulate matter and in sediments (Wakeham et al., 1997).

3.6.5. Terrestrial inputs

Contributions of terrestrial organic matter to sediments at APEI-6 SW were evident from a number of compound classes and ratios. High molecular weight fatty acids, *n*-alkanes and alcohols were all present in the sediments. The *n*-alkanes were dominated by the C_{29} homologue

(ACL = 29), with the C_{31} homologue being the next most prevalent alkane. The carbon preference index (CPI) of n-alkanes averaged ~ 7.5; this, combined with an ACL of C_{29}, is a clear indication of a contribution of higher plant waxes to the sediments (Brassell and Eglinton, 1983). Similarly, high molecular weight (HMW) fatty acids yielded a mean CPI of ~ 6, suggesting the source of HMW fatty acids is from higher-plant derived organic matter (Gagosian and Peltzer, 1986; Kawamura et al., 2003; Ohkouchi et al., 1997). This has been previously documented for sediments in the Pacific despite the distance from land, with the dominant mechanism of transport for this soil- and plant-derived terrestrial organic matter ascribed to aerosols (Gagosian and Peltzer, 1986; Kawamura et al., 2003; Ohkouchi et al., 1997).

A high abundance of C_{27}, C_{29}, C_{31} n-alkanes of terrestrial origin was also observed in the APEI-6 SW and UK-1 nodules collected by trawl on JC120 (expanded in Shulga, 2018). The CPI ~ 3 in nodules indicates the presence of more biodegraded organic matter compared to underlying sediments. High concentrations of C_{16}, C_{18}, C_{20} n-alkanes and iso-, anteiso- C_{16} fatty acids associated with microbial degradation of organic matter confirm the occurrence of active bacterial processes within the nodules (Shulga, 2018). These differences in biogeochemistry may help explain the differences in bacterial community structure between the nodules and sediments observed in APEI-6 NE, OMS and UK-1 samples (Lindh et al., 2017).

3.7. Biological composition

3.7.1. Bacteria and Archaea

Branched fatty acids, generally indicative of anaerobic bacteria, accounted for 1–14% of the total surface sediment lipid pool at APEI-6 SW (Gillan and Johns, 1986). Hopanoids, mainly indicative of aerobic bacteria, accounted for 3–16% of the total lipid pool at APEI-6 SW (Ourisson and Rohmer, 1992). Arachidonic acid, $C_{20:4(n-6)}$ was the dominant PUFA in the sediments at APEI-6 SW, constituting ~ 40% of the PUFA pool. This fatty acid has been linked to piezophilic bacteria (Fang et al., 2004; Fang et al., 2006) and is present in high concentrations in some echinoderms (Drazen et al., 2008; Howell et al., 2003; Jeffreys et al., 2009b; Mansour et al., 2005).

Environmental metabarcoding (described in the rest of the section) of 30 sediment samples from the APEI-6 SW area yielded a total of 12,836 bacterial and archaeal OTUs (operational taxonomic units; sharing 99% sequence identity) from 153,000 16S rRNA gene sequences (expanded in Hollingsworth et al., 2021). Of these OTUs, 20.23% were classified as Archaea, 79.34% as Bacteria and 0.43% could not be assigned to domain level (Unassigned).

Across all studied abyssal plain sites of the APEI-6 SW and UK1 contract area, sediment microbial assemblages were dominated by members of the Thaumarchaeota, Alphaproteobacteria, Gammaproteobacteria and Planctomycetes. The *Nitrosopumilus* genus in the archaeal Thaumarchaeota group were enriched in the sediments. Members of the Thaumarchaeota group are chemolithoautotrophic nitrifiers, capable of oxidising ammonia (Könneke et al., 2005). The genus *Nitrospira* (2% relative abundance of sequences) is capable of nitrite oxidisation (Koch et al., 2015) and has been previously reported in similar proportions in CCZ sediments (Shulse et al., 2017)

As a group, the Proteobacteria represented the largest proportion of the sediment microbial assemblages at APEI-6 SW and UK1, followed by the Thaumarchaeota. Both showed variation between sites at APEI-6 SW and UK1. Thaumarchaeota formed a higher proportion of the community in the deeper sediment layers (20–22 cmbf) at APEI-6, whilst at UK1, this group was more abundant in the top two centimetres in the JC120 data. Other major groups also displayed spatial variation through the sediment. Actinobacteria, Bacteroidetes, Deltaproteobacteria, Gammaproteobacteria and Nitrospirae were more enriched in the 0–6 cmbf fraction of sediments at both the APEI-6 SW and UK1 sites. Chloroflexi were also more abundant in surface sediments across APEI-6 SW, but not at UK1, where the reverse pattern was observed. Conversely, some groups were more abundant in deeper sediment fractions at both sites, such as Cyanobacteria and Betaproteobacteria in the 10–12 cmbf and 20–22 cmbf layers. Cyanobacterial OTUs occurred in very low relative abundance in the top 0–6 cmbf of sediment at all sites. These cyanobacteria comprised the *ML635J-21* lineage within the Melainabacteria class, a group of non-photosynthetic cyanobacteria (Soo et al., 2014).

3.7.2. Macrofauna

The macrofauna (some common representatives are shown in Fig. 5) was dominated by annelids and isopod crustaceans noted elsewhere in the CCZ (Glover et al., 2002; Hessler and Jumars, 1974; Janssen et al., 2019; Paterson et al., 1998). Although the foraminifera are typically abundant in the CCZ (Gooday et al., 2015; Mullineaux, 1987; Veillette et al., 2007a), these have not been studied systematically in APEI-6 samples. Data are therefore limited to the metazoan component. Macrofaunal abundance was dominated by crustaceans, sponges, annelids, cnidarians, molluscs, and others (including Brachiopoda, Chaetognatha, Chordata, Nematoda, Platyhelminthes and unidentified taxa). The most common macrofaunal species in APEI-6 SW was the sponge *Plenaster craigi* Lim & Wiklund, 2017 (expanded in Taboada et al., 2018), a demosponge originally described from the OMS contract area, adjacent to UK-1 (Lim et al., 2017). Mean densities of 12 ± 6.2 individuals m^{-2} observed for the sponge across APEI-6 SW, corroborates the suggestion that *P. craigi* might be the most common sessile metazoan occurring in the CCZ (Lim et al. 2017). In APEI-6 SW, *P. craigi* density was positively correlated to the number of nodules. We detected molecular affinities between samples of *P. craigi* from APEI-6 SW and UK1 Stratum A, despite a separation of ~ 800 km. Migration analysis in Taboada et al. (2018) inferred very little progeny dispersal of individuals between areas and hydrodynamic models suggested a prevalent northeasterly transport trajectory, i.e., from exploration contract areas to APEI-6 SW.

A total of 16 macrofaunal (infauna and encrusting fauna) taxa from six phyla (Annelida, Bryozoa, Echinodermata, Mollusca, Porifera and Sipuncula; note that the Arthropoda were present but not processed) were confirmed with both morphological and molecular data to occur in both APEI-6 boxcores and UK1 exploration contract areas (Table S6). These data indicate species ranges of ~ 500 km (i.e. across APEI-6 SW and NE sites) and between APEI-6 and UK1 exploration areas separated by ~ 1000 km. An additional 24 taxa were only detected in APEI-6 NE. Investigation of the population-level connectivity of the widespread species based on sequences from additional individuals is ongoing (Dahlgren et al. in prep.).

These data allow the first test of the hypothesis of Glover et al (2002) that there is a core group of abundant, widespread species that can range

Fig. 5. Microscope images of macrofauna. Upper row from left to right: Aplacophora indet, *Anguillosyllis* sp., *Ledella* sp., Echinodermata juvenile indet., *Aglaophamus* sp., Bryozoa indet. Middle row from left to right: Bryozoa indet., *Glycera* sp., *Ophelina martinezarbizui* Wiklund et al., 2019, Gastropoda indet., Sphaerodoridae indet., *Laonice* sp. Lower row from left to right: *Dacrydium* sp., Flabelligeridae indet., *Myonera* sp., *Plenaster craigi* Lim & Wiklund, 2017.

freely across the eastern tropical Pacific abyssal plain at scales of at least 1000 km. This hypothesis is now supported by some molecular evidence. However, it is not yet possible to ascertain degrees of endemism, if any, at particular sites, as all sites (in particular the APEI-6) are under sampled. The presence of 24 taxa only detected in APEI-6 is suggestive of some degree of turnover (Paterson et al., 1998) but given the level of under sampling, they cannot be described as 'endemic' to the APEI-6 region. In addition, studies (Stewart et al in prep) of an additional ~ 3000 specimens from the UK1 and OMS regions reveal many taxa that are not found in APEI-6, with probably many absences owing to under sampling of APEI-6. The general pattern is in agreement with a molecular-only study of the BGR and IFREMER exploration areas (Janssen et al., 2015), in which 95 out of 233 polychaete molecular operational taxonomic units (MOTUs) were shared across distances of 1300 km, but perhaps differs from their finding that just two out of 95 isopod MOTUs were shared across that distance. Common polychaetes and isopods showed molecular connectivity among populations between the IFREMER and BGR exploration areas of all species investigated (Janssen et al., 2019), although they inferred weak barriers to gene flow for the isopod species, probably related to the fact that the species under study are brooders and hence have limited dispersal abilities. In a recent study of harpacticoid copepod species ranges based on molecular data from the US continental margin (Easton and Thistle, 2016), a relatively small number (13.3%) of broadly-distributed (1000 km or more) species were found. The more restricted ranges for isopods and copepods respectively may arise from a lack of pelagic larval dispersal (Easton and Thistle, 2016; Janssen et al., 2015). The only data on larvae from APEI-6 are from a single plankton pump sample (incorrectly labelled as APEI-4), which obtained 2 individual meroplankton, both larval polychaetes of the same morphotype (OTU 21) (Kersten et al., 2017).

Our preliminary data suggest that APEI-6 shares a significant number of macrofaunal taxa with nearby exploration contract areas. However, molecular-based data on species ranges, as well as information on population connectivity, is needed for many more taxa and over more than just one of the nine APEIs to inform evaluation of ecosystem resilience. This is unlikely to happen without the adoption of a consistent DNA-based taxonomy of species recorded from the CCZ (Glover et al., 2016a).

3.7.3. Scavengers (crustaceans and fishes)

Trap catches at APEI-6 SW were large and comprised 8,201 amphipods all of which were resolved to the species level (Table S7). The species composition of the two traps from APEI-6 SW were similar with nine of the total twelve species recorded in both sets of traps. The abyssal amphipod scavenger community is a mobile fauna with some species recorded globally (Horton et al., 2020b; Thurston, 1990). However, improved characterisation of mobile scavenger populations using molecular tools has revealed that species once believed to be cosmopolitan are in fact closely-related species complexes (d'Udekem d'Acoz and Havermans, 2015; Havermans, 2016; Havermans et al., 2013; Horton et al., 2020a). Our results on the molecular barcoding of voucher specimens using CO1 allowed us to confirm the identification of the species in Table S7. Both our molecular analyses and recent publications indicate that cryptic speciation may occur in the genera *Eurythenes* and *Paralicella* (Havermans, 2016; Ritchie et al., 2015), the largest bodied and the dominant taxa in abyssal traps respectively. Remarkably, we found three new species in the genera *Cyclocaris, Paracallisoma* and *Haptocallisoma* (Table S7), which will be described elsewhere. The trap also captured the zoarcid fish *Pachycara nazca* Anderson & Bluhm 1997 and an unidentified penaeid shrimp. Baited trap samples in APEI-6 NE contained three species of scavenging amphipods *Paralicella caperesca* Shulenberger & Barnard 1976, *Paralicella tenuipes* Chevreux 1908 and *Cyclocaris* sp. DISCOLL.CCZ.JC120.008.1 (Mohrbeck et al., 2021).

The single baited camera deployment in APEI-6 NE observed the fish *Coryphaenoides* spp. (either or both of *C. armatus* (Hector 1875) and *C. yaquinae* Iwamoto & Stein 1974), the shrimp *Cerataspis monstrosus* Gray 1828 sp. inc. (formerly *Plesiopenaeus armatus* (Spence Bate 1881)) and *Hymenopenaeus nereus* (Faxon 1893) sp. inc., and the brittle star *Ophiosphalma* cf. *glabrum* (Lütken & Mortensen, 1899) (formerly *Ophiomusium glabrum* Lütken & Mortensen 1899). These taxa were all common in the UK1 license areas but the total scavenger species richness in APEI-6 NE was much lower than in those other areas. Regional variation in the scavenging community is apparent from across the CCZ (Drazen et al., 2021). However, in this case, a single deployment was inadequate to fully characterize the fauna in APEI-6 (Leitner et al., 2017).

3.8. Megafauna

3.8.1. Metazoa

Megafauna (metazoans > 1 cm) across APEI-6 SW (Fig. 6) were dominated by soft corals and anemones (Order Alcyonacea: 32.8% of total abundance; Order Actiniaria: 11.7 %), sponges (Class Demospongiae: 10.1%; Class Hexactinellida: 1.3%; Porifera indet.: 7.1%), echinoderms (14.6 %), bryozoans (11.3%), and arthropods (Subphylum Crustacea: 7.4%). Fishes, tunicates, annelid worms and ctenophores were also found in much lower proportions (<1.5% each). From all the metazoans detected, 76% were suspension feeders, 15% were deposit feeders, and 9% were predators and scavengers. Most of the metazoan megafauna encountered in APEI-6 SW (56.1%) were found growing on polymetallic nodules or on other hard substrata, as appears to be common in eastern CCZ megabenthic communities (Amon et al., 2016; Simon-Lledó et al., 2019b; Simon-Lledó et al., 2020).

Mean metazoan density at APEI-6 SW (expanded in Simon-Lledó et al., 2019a) was 0.38 ind. m^{-2}, and showed a patchy distribution, ranging from 0.19 to 0.51 ind. m^{-2} with different morphotypes being proportionally abundant (across the 12 transects surveyed; summarised in Table 3). Faunal density in APEI-6 was substantially higher than those reported in TOML areas B and C (0.11 – 0.14 ind. m^{-2}), similar to that found in TOML D site (0.44 ind. m^{-2}), but much lower than that encountered at UK1 (1.08 ind m^{-2}) in methodologically comparable studies (Amon et al., 2016; Simon-Lledó et al., 2020).

Locally, faunal density and assemblage composition appeared to be correlated with geomorphological variations at broader scales (tens of km; Table S1; (expanded in Simon-Lledó et al., 2019a)), while nodule coverage was related to these parameters at fine scales (tens of metres). Nodule-free areas exhibited a substantially lower density and a different assemblage composition (expanded in Simon-Lledó et al., 2019b). Nodule density may not be independent of the local seabed morphology but no simple relationship has been found elsewhere in the CCZ between these factors (Mewes et al., 2014; Peukert et al., 2018). Higher nodule coverage at the seafloor has been commonly related with higher megafauna densities across the CCZ (Radziejewska and Stoyanova, 2000; Simon-Lledó et al., 2020; Vanreusel et al., 2016). Nodules provide hard substratum for sessile taxa (e.g. suspension feeding cnidarians and sponges) that seem to dominate the metazoan megafaunal assemblages in the eastern CCZ (Amon et al., 2016; Simon-Lledó et al., 2020; Vanreusel et al., 2016). The spatial variability in both geomorphological variation and nodule densities (Simon-Lledó et al., 2019a; Simon-Lledó et al., 2019b), likely as well as other uninvestigated factors, corresponds with relatively high heterogeneity in the megafauna even within the APEI-6 SW area assessed.

A total of 123 invertebrate and eight fish morphotypes were identified among the 7116 megafauna specimens detected in APEI-6 SW during AUV surveys (expanded in Simon-Lledó et al., 2019a). These morphotypes are as near to species identifications as can be made from these images, although they may under or over-estimate true species composition. The Echinodermata was the most species-rich phylum in APEI-6 SW, with a total of 33 morphotypes observed, followed by the Porifera (30 morphotypes) and the Cnidaria (27 morphotypes). Examination of the photographs from APEI-6 NE detected 40 invertebrate morphotypes (note > 5 cm minimum dimension at APEI-6 NE, rather

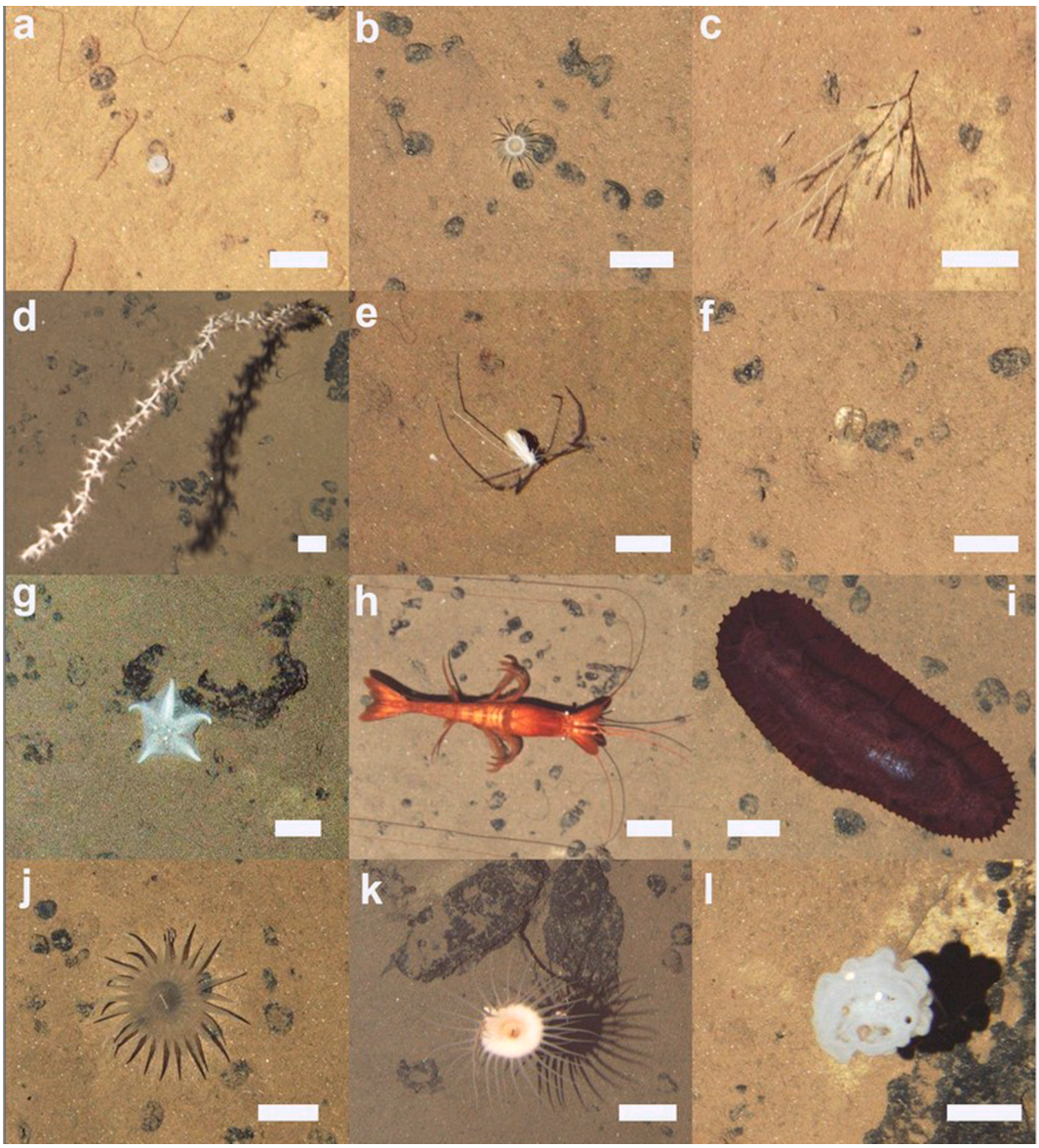

Fig. 6. Examples of seafloor metazoan megafauna photographed at the abyssal plain sites of APEI-6 SW during AUV survey. Scale bars representing 5 cm. CCZ-standardised megafauna morphotype (mtp) codes in capital letters. a to f: Abundant taxa (density = 50–400 ind. ha^{-1}) . g to l: Scarce taxa (density < 5 ind. ha^{-1}). a) Demospongiae indet. mtp-POR_002, higher density in areas with low nodule abundance. b) Actiniaria stet. mtp-ACT_022 and c) Farciminariidae indet. mtp-BRY_005, higher density in areas with mid nodule abundance. d) *Lepidisis* gen. inc. mtp-ALC_005, higher density in areas with mid to high nodule abundance. e) Munnopsididae indet. mtp-ART_001 and f) Spatangoida indet. mtp-URC_012. g) *Hymenaster pellucidus* sp. inc. (AST_012) h) *Cerataspis monstrosus Gray, 1828* sp. inc. (DEC_001). i) *Benthodytes* indet. mtp-HOL_037. j) Actiniaria stet. mtp-ACT_010. k) Metridioidea stet. mtp-ACT_042. l) *Saccocalyx pedunculatus* sp. inc. (HEX_020).

than the > 1 cm minimum dimension used in the analysis of APEI-6 SW) and six fish taxa, all of which were shared with the SW except for two holothurian morphotypes. Note that the APEI-6 NE images were not as high quality or analysed in as much detail as the APEI-6 SW images and no quantification was made of faunal densities. Almost half (48%) of the invertebrate morphotypes (>1 cm) found in APEI-6 (NE and SW sites combined) were also encountered at the UK1 area (reassessed from Amon et al 2016) where a total of 110 morphotypes were identified from the 4470 invertebrate specimens detected in quantitative image surveys. The assemblages of these two areas also substantially differed in the relative abundance of several of the dominant taxonomic groups. For instance, sponges and soft corals were respectively 2 and 4 times more abundant in UK1, while the density of anemones was 3 times higher in APEI-6 study areas. Most remarkably, among the mobile fauna, echinoid (sea urchins) abundance was almost twice as high in APEI-6 than at UK1. Densities of asteroids (sea stars) and ophiuroids (brittle stars) were 35 and 15 times higher respectively at UK1 than at APEI-6. While further regional synthesis work is needed to better understand biogeographical variations across the CCZ and within the APEI-6 and UK-1 areas, preliminary comparisons of the APEI-6 megafauna with other areas (e.g. Simon-Lledó et al., 2020; this study) suggest a low similarity (and thus potentially low representativity) of the megabenthic assemblages of this protected area compared to areas studied in UK1 and TOML contract areas.

3.8.2. *Protista*

Xenophyophores (giant foraminifera) are exceptionally diverse in the CCZ (Gooday et al., 2020a; Gooday et al., 2017b). Nine species were recognised in samples collected in APEI-6 NE during AB02. In seafloor photographs from APEI-6 SW, the mean density of xenophyophores was 2.59 ind. m^{-2} (CI_{95} ± 0.79) but values varied across the region (Table S3), with maximum recorded densities per image reaching 17

ind. m^{-2}. >75% of all those recognised could be identified as *Aschemonella monilis* Gooday & Holzmann 2017 (30,525 individuals), a species recently described from the UK1 contract area (Gooday et al., 2017a) that has a genetically confirmed range spanning 3,800 km from the UK1 contract areas in the east to APEI-4 in the west (Gooday et al., 2020a; Gooday et al., 2020b). The abundance of xenophyophores in APEI-6 appears to be higher than in other image-based analyses along the CCZ. In comparison, average densities were 0.16. ind. m^{-2} in the Eastern CCZ JSC Yuzhmorgeologiya contract area (although the maximum density recorded in a single picture reached 12 ind. m^{-2}) (Kamenskaya et al., 2013) and 0.65 ind. m^{-2}. in the UK1 contract area (Amon et al., 2016). Xenophyophores seen in pictures from APEI-6 SW were classified into 23 morphotypes, but real diversity could be much higher, as it may be difficult to discriminate between species based on seafloor images (Gooday et al., 2018).

3.9. Fossils and other observations

Fossils were abundant across APEI-6 SW (Table S3), especially within the ridge area where fossil shark teeth alone had average densities of (1085 ± 905.1 ha^{-1}). Identifiable fossils in pictures ranged from 5 to 50 cm length, and were mainly composed of: i) mezorostral and maxillar bones of ziphioid whales; and ii) *Otodus megalodon* (Agassiz 1843), *Hemipristis* sp, and *Oxyrhina* sp. shark teeth, similar to those collected during pioneer expeditions to the CCZ (Thomson and Murray, 1895). Large-sized fossils are known to be common across the CCZ seafloor (Heezen and Hollister, 1971; Smith, et al., 2019; Smith et al., 2015b), but we present the first density data (Table S3).

Paleodictyon is an important group of traces with a hexagonal structure, found globally in fossilised sediments and multiple deep-sea locations. Modern traces corresponding with *Paleodictyon nodosum* were commonly found on the APEI-6 seafloor (average density 0.33 ind. m^{-2}; mean size 45 mm; (Durden et al., 2017);Table 3).

3.10. An APEI-6 SW seamount

3.10.1. Morphology of seamounts in APEI-6

The seamounts (>1000 m elevation) and knolls (200–1000 m elevation) mapped in APEI-6 are mostly circular in shape and vary widely in size (0.7 – 9.3 km across, 150 – 1000 m high; Fig. 1). Global bathymetry data indicate a total of nine seamounts and 49 knolls in the whole of APEI-6 (Washburn et al., 2021). Most have relatively flat tops, in some cases with a prominent cone and central crater. Some of the smaller seamounts have a ring-shaped morphology. The single seamount surveyed as part of this study is the tallest feature in the APEI-6 SW area, reaching 1000 m above the surrounding seafloor. Its flanks are steep, reaching slopes up to 35°, but at the 50-m-pixel resolution of our bathymetric dataset, they appear relatively smooth. The seamount is topped by a large volcanic cone that covers nearly the entire structure, featuring a large crater around 1200 m across and 100 m deep. The edge of the crater is rocky (Fig. 7) and steep and some areas have vertical walls.

3.10.2. Visual appearance of seafloor at an APEI-6 SW seamount

The observed seamount seafloor was predominantly composed of pillow basalts with a very thin Fe-Mn crust coating (Fig. 3e and 7). The amount of finer sediment was variable, ranging from totally absent on exposed bedrock sections, to full sediment coverage in patches at the centre of the caldera (30.2 % of total area surveyed by video). Variably-sized talus fragments occurred on generally sediment-covered patches: large (>50 cm) detached rocks were common beneath the caldera flanks, whereas boulders (>256 mm), cobbles (256 < 64 mm), and pebbles (64 > 4 mm) were rather patchily distributed across the crater.

3.10.3. Sediment composition at an APEI-6 SW seamount

A single megacore deployment was made at the seamount summit. The appearance of the core samples was quite distinct from elsewhere. In the top 300 mm of Megacore samples there were three layers of differing

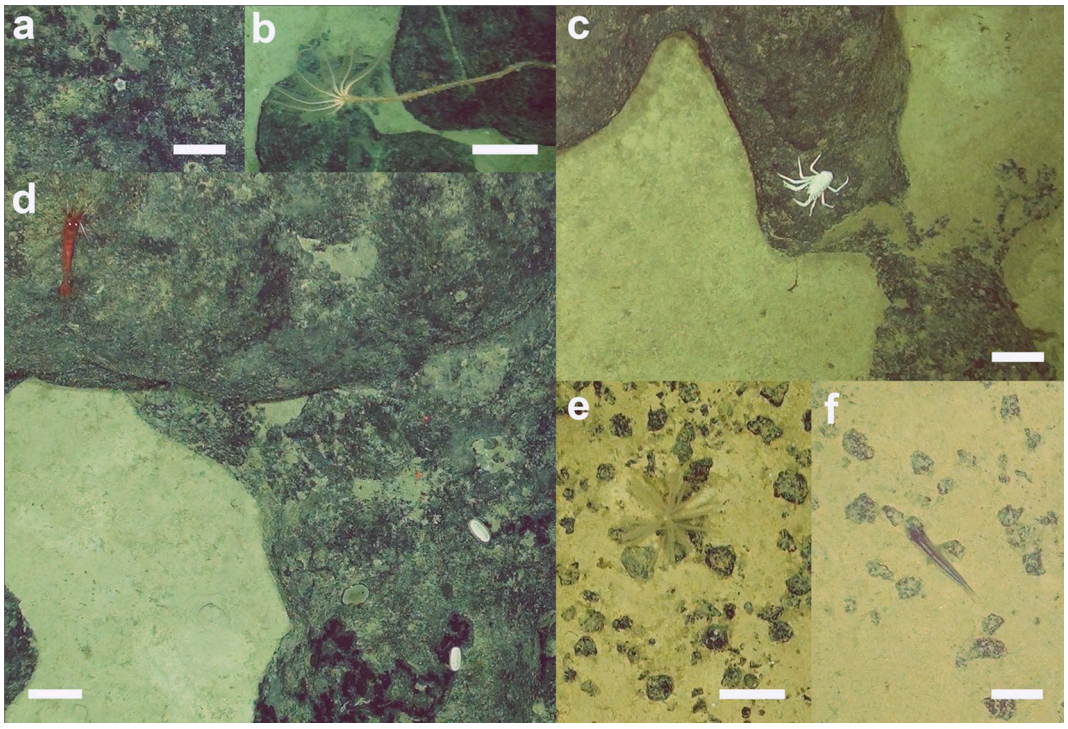

Fig. 7. Examples of metazoan megafauna photographed at the seamount of APEI-6 SW during AUV survey. CCZ-standardised megafauna morphotype codes in capital letters. Scale bars represent 10 cm. a to d: crater flanks. e and f: centre of crater. a) *Hymenaster* indet. mtp-AST_017. b) *Bathymetrina* indet. mtp-CRI_001. c) *Munidopsis* indet. mtp-DEC_007. d) top-left: *Nematocarcinus* indet. mtp-DEC_005, bottom-right: Leptochitonidae indet. mtp-MOL_002. (e) Cladorhizidae stet. mtp-DES_005. f) *Bathytyphlops sewelli* sp. inc. (Ipnopidae).

colour. In the seamount crater, surface sediments were calcareous and composed primarily of coccoliths. As a result, they were much paler in colour than sediments in the rest of the APEI-6 SW sites. These paler sediments appeared from the video data to be broadly representative of the seamount crater. The seamount crater sediments had very low levels of TOC and TN but high levels of $CaCO_3$. Similar coloured sediments were also observed on seamount summits in APEI-1, 4 and 7 (Laroche et al., 2020; Leitner et al., 2020). Below the light-coloured surface sediments of the APEI-6 SW seamount investigated, there was a distinct darker brown layer of unknown composition.

The grain size in the paler coloured sediment samples from the seamount summit (top 100 mm of the core) were much coarser than elsewhere. The grain sizes showed a bimodal distribution, with peaks at: i) 7.2 μm, as observed in plain locations, and ii) 57.74 μm. A similar bimodal pattern in surface sediments occurred at the KODOS site (western CCZ), with a coarse (50–60 μm) and a fine mode (2–8 μm) (Jung et al., 1998). As the analysis presented here is based on a single core deployment, it is unclear how representative these data are.

3.10.4. Seamount microbes at an APEI-6 SW seamount

Microbial communities in the seamount crater sediments were distinct from those sampled at other APEI-6 SW and UK1 sites. The relative abundance of Thaumarchaeota in the seamount sediments was half that of the APEI-6 and UK1, with a marked reduction (27%) in the 20 cmbf layer. The deeper layers of the seamount crater sediment were dominated by Cyanobacteria (>50%), which showed a six-fold increase in relative abundance compared to the other sites within the APEI-6 and UK1. Likewise, the relative abundance of Betaproteobacteria exhibited a ten-fold increase in the 10–20 cmbf layers of the crater sediment.

3.10.5. Seamount megafauna at an APEI-6 SW seamount

A total of 37 metazoan morphotypes were found in images obtained at the seamount. Of these, 25 were also found across abyssal plain sites, whereas 12 were only recorded on the seamount transect (all of these inhabited exposed bedrock). Three of these morphotypes accounted for almost 60% of all fauna observed on the APEI-6 SW seamount. These were: a starfish (*Hymenaster* indet. mtp-AST_017: 40%), a soft coral (Primnoidae indet. mtp-ALC_038: 11%), and a chiton (*Leptochitonidae* indet. mtp-MOL_002: 7%). Two decapods, also found at plain sites, comprised the remainder of the top five most abundant morphotypes at the seamount: a shrimp (*Nematocarcinus* indet. mtp-DEC_005: 4%), and a squat lobster (*Munidopsis* indet. mtp-DEC_007: 3%). A broadly similar suite of faunal groups were also seen at seamounts at APEI-3 (Cuvelier et al., 2020)

The numerical density of megafauna recorded on the seamount transect was a fifth of that at the other APEI-6 SW sites. Note, however, that the above-seabed altitude of image collection was higher in the seamount survey, which possibly constrained the detection of the smallest megafauna. Sections where exposed bedrock was visible hosted a higher metazoan abundance, 27% more than areas with full sediment coverage, because of a higher density of hard substratum epifauna (63% of all individuals identified).

4. Conclusions

We summarise a wide variety of multidisciplinary information for APEI-6, including new data and syntheses of more detailed studies already published. Despite representing only a small percentage (~4%) of the total area of APEI-6, the areas visited to date exhibit obvious heterogeneity in many parameters. APEI-6 has a variable landscape-scale morphology and images of the seafloor encompass a wide range of habitats, from steep rocky areas, through coarse-sediment flats in the seamount caldera, to flat, fine-grained abyssal plain sediments. Nodules are generally small but variable in density across a range of spatial scales. The fine sediment comprising much of the seafloor, excluding the seamount, is less variable, with consistent grain sizes, composition and biochemical properties. All the oceanographic parameters assessed are spatially similar, although some depth-related trends are detectable.

The small areas sampled in APEI-6 have some similarities but also important differences compared to the nearest exploration contract areas in the CCZ. APEI-6 has a similar range of depths and broadly similar morphology to much of the eastern CCZ, with ridges, troughs, flatter plains and knolls/seamounts. The oceanographic conditions are similar, although there were some differences in deep water-mass separation between APEI-6 and UK-1 study areas. The most striking difference between APEI-6 SW and the exploration contract areas studied was in the polymetallic nodule resource. The nodules in APEI-6 SW are generally smaller and cover less seabed than in the exploration areas, although the nodules can reach high numerical densities at APEI-6 SW. Nodule sizes and abundances are also highly variable within contract areas (e.g. Simon-Lledó et al., 2020). The nodule composition appear different, with APEI-6 SW nodules having lower concentrations of metals, such as Mn. The non-nodule sediments from APEI-6 SW have a similar grain size and composition to contract areas. Much of the biogeochemistry was also comparable, except for oxygen penetration depths, which were shallower in the exploration contract areas.

The faunal communities of APEI-6 SW were surprisingly variable, with heterogeneity in most of the assemblages investigated. This faunal variability may be associated with landscape-scale patterns (Simon-Lledó et al., 2019a) and nodules variability (Simon-Lledó et al., 2019b), but also reflects under-sampling of fauna occurring at low densities (Ardron et al., 2019). Mobile scavengers seem to be less variable, although they were also under sampled. Many aspects of the ecology of the areas were similar, notably for bacterial and scavenger assemblages. Megafauna and (to the extent determinable) macrofauna exhibit some differences in density, diversity and community structure, although more than half the species are shared with eastern CCZ contract areas investigated. The initial information on the megafauna from APEI-3 suggests this area is also different to both APEI-6 and the contractor areas (Cuvelier et al., 2020; Vanreusel et al., 2016) but this is based on very limited survey extents at APEI-3.

Our view is that the area studied in APEI-6 is partially representative of the exploration areas to the south, yet the study sites show distinct differences in a number of key aspects. It is important to note that the areas studied may not represent the entire APEI-6. Clearly, substantially more information across the entire APEI-6, and other APEIs, is needed to evaluate their representativity. From a management perspective, caution has to be exercised when assuming that this APEI can fully contribute to the APEI network in its role of regional conservation and "Protect biodiversity and ecosystem structure and function by a system of representative seafloor areas closed to mining activities" (International Seabed Authority, 2011). The lack of large abundant nodules and the habitats they create in our APEI-6 study areas, if they are representative of the entirety of APEI-6, suggests a potentially important difference to many of the eastern CCZ mining contract areas. If APEI-6 doesn't include the habitat that is specifically targeted by mining activities additional APEIs (McQuaid et al., 2020) or other management activities, beyond the APEI network alone, are warranted in order to mitigate the impacts of mining development in the eastern CCZ.

Although the information presented here on APEI-6 is broad and multidisciplinary, it comes from a restricted area of the APEI and there are gaps in understanding that will limit assessment of the extent to which the APEI network fulfils its intended purpose. In particular, we now know that abyssal regions are highly variable over a broad range of spatial scales (Smith et al., 2020), so well designed stratified sampling programs using comparable methods will be extremely important in order to evaluate the ecology and biogeography of the CCZ. Key knowledge gaps include: water-column biology, water flow and connectivity between areas, soundscapes, reproduction, meiofauna (foraminifera and metazoan), megafaunal biodiversity (species-level from specimens), faunal interactions (including trophic structure, behaviours), and the functioning of species (key roles, e.g. bioturbation) and

ecosystems (fluxes, production, etc.). Natural temporal variability in the physical and biological environment is unstudied, as are existing anthropogenic impacts to the CCZ. The seamounts of APEI-6 and their fauna have not been well characterised but the initial assessment of one seamount presented here suggests their potential distinctiveness. It is also notable that one of the key criteria for determining the location of the APEIs (International Seabed Authority, 2011), the fracture zone that runs through the middle of APEI-6, has never been investigated despite its potential for hosting additional ecosystems (Riehl et al., 2020). A mechanism, potentially introduced by the ISA (Lodge et al., 2017), is needed to encourage additional investigation of the APEI network to ensure it can maintain its role as the contractor areas are increasingly understood.

This study advances the state of knowledge of one of the nine APEIs in the CCZ and improves understanding of the extent of its representativity in a range of important environmental parameters. This information is critical for effective regional-scale management of the CCZ and should inform the next revision of the International Seabed Authority Environmental Management Plan for the CCZ (International Seabed Authority, 2011). We also hope that this research stimulates further interest in the APEI network and encourages their study. Alongside the increasing focus on the exploration contract areas, there needs to be a mechanism to fund equivalent research and monitoring in the APEIs.

Data Accessbility Statement

The data supporting the findings of this study are available within the article, its supplementary materials or in referenced publications.

Declaration of Competing Interest

The authors declare that they have no known competing financial interests or personal relationships that could have appeared to influence the work reported in this paper.

Acknowledgements

We would like to express our thanks to the masters and crews of RRS *James Cook*, RV *Thomas G Thompson* and RV *Melville* for the successful operations at sea. We would like to thank James Bell and Pierre Josso for assistance with sampling. Thanks to Emma Critchley for taking the images of the nodules. Thanks to Steve Persall from UK Seabed Resources Ltd. for help in extracting historical data. Thanks to Malcolm Clark and one anonymous reviewer for constructive comments that improved the manuscript. The research leading to these results has received funding from the European Union Seventh Framework Programme (FP7/2007-2013) under the MIDAS (Managing Impacts of Deep-seA reSource exploitation) project, grant agreement 603418. This work was part of the NERC Seabed Mining And Resilience To EXperimental impact (SMARTEX) project (Grant Reference NE/T003537/1). This work was also supported by the NERC National Capability funding to the National Oceanography Centre, as part of the Climate Linked Atlantic Section Science (CLASS) program (Grant Reference NE/R015953/1). The ABYSSLINE (ABYSSal baseLINE) environmental survey was supported by a collaborative partnership between six non-profit global academic research institutes (University of Hawaii at Manoa, Natural History Museum, Uni Research (now NORCE), the UK National Oceanography Centre, Senckenberg Institute, IRIS Norway) and funded by UK Seabed Resources Ltd. Funding was also provided by the Swedish Research Council FORMAS and Joint Programming Initiative Healthy and Productive Seas and Oceans (JPI Oceans). The funders had no role in data collection, analysis or write-up of results.

Appendix A. Supplementary data

Supplementary data to this article can be found online at https://doi.org/10.1016/j.pocean.2021.102653.

References

Alevizos, E., Huvenne, V.A.I., Schoening, T., Simon-Lledo, E., Robert, K., Jones, D.O.B., submitted. Linkages between sediment thickness, geomorphology and Mn nodule occurrence: new evidence from AUV geophysical mapping in the Clarion-Clipperton Zone.

Aleynik, D., Inall, M.E., Dale, A., Vink, A., 2017. Impact of remotely generated eddies on plume dispersion at abyssal mining sites in the Pacific. Scientific Reports 7 (1), 16959.

Amon, D., Ziegler, A., Kremenetskaia, A., Mah, C., Mooi, R., O'Hara, T., Pawson, D., Roux, M., Smith, C., 2017a. Megafauna of the UKSRL exploration contract area and eastern Clarion-Clipperton Zone in the Pacific Ocean: Echinodermata. Biodiversity Data Journal 5.

Amon, D.J., Ziegler, A.F., Dahlgren, T.G., Glover, A.G., Goineau, A., Gooday, A.J., Wiklund, H., Smith, C.R., 2016. Insights into the abundance and diversity of abyssal megafauna in a polymetallic-nodule region in the eastern Clarion-Clipperton Zone. Scientific Reports 6, 30492.

Amon, D.J., Ziegler, A.F., Drazen, J.C., Grischenko, A.V., Leitner, A.B., Lindsay, D.J., Voight, J.R., Wicksten, M.K., Young, C.M., Smith, C.R., 2017b. Megafauna of the UKSRL exploration contract area and eastern Clarion-Clipperton Zone in the Pacific Ocean: Annelida, Arthropoda, Bryozoa, Chordata, Ctenophora, Mollusca. Biodiversity Data Journal 5.

Amos, A.F., Roels, O.A., 1977. Environmental aspects of manganese nodule mining. Marine Policy 156–163.

Ardron, J.A., Simon-Lledó, E., Jones, D.O.B., Ruhl, H.A., 2019. Detecting the Effects of Deep-Seabed Nodule Mining: Simulations Using Megafaunal Data From the Clarion-Clipperton Zone. Frontiers in Marine Science 6 (604).

Bau, M., Schmidt, K., Koschinsky, A., Hein, J., Kuhn, T., Usui, A., 2014. Discriminating between different genetic types of marine ferro-manganese crusts and nodules based on rare earth elements and yttrium. Chemical Geology 381, 1–9.

Brassell, S.C., Eglinton, G., 1983. The potential of organic geochemical compounds as sedimentary indicators of upwelling. In: Suess, E., Thiede, J. (Eds.), Coastal Upwelling, Its Sedimentary Record. Plenum Press, New York, pp. 545–571.

Brenke, N., 2005. An Epibenthic Sledge for Operations on Marine Soft Bottom and Bedrock. Marine Technology Society Journal 39 (2), 10–21.

Caporaso, J.G., Kuczynski, J., Stombaugh, J., Bittinger, K., Bushman, F.D., Costello, E.K., Fierer, N., Peña, A.G., Goodrich, J.K., Gordon, J.I., Huttley, G.A., Kelley, S.T., Knights, D., Koenig, J.E., Ley, R.E., Lozupone, C.A., McDonald, D., Muegge, B.D., Pirrung, M., Reeder, J., Sevinsky, J.R., Turnbaugh, P.J., Walters, W.A., Widmann, J., Yatsunenko, T., Zaneveld, J., Knight, R., 2010. QIIME allows analysis of high-throughput community sequencing data. Nature Methods 7 (5), 335–336.

Caporaso, J.G., Lauber, C.L., Walters, W.A., Berg-Lyons, D., Huntley, J., Fierer, N., Owens, S.M., Betley, J., Fraser, L., Bauer, M., Gormley, N., Gilbert, J.A., Smith, G., Knight, R., 2012. Ultra-high-throughput microbial community analysis on the Illumina HiSeq and MiSeq platforms. The ISME Journal 6 (8), 1621–1624.

Caporaso, J.G., Lauber, C.L., Walters, W.A., Berg-Lyons, D., Lozupone, C.A., Turnbaugh, P.J., Fierer, N., Knight, R., 2011. Global patterns of 16S rRNA diversity at a depth of millions of sequences per sample. Proceedings of the National Academy of Sciences 108 (Supplement 1), 4516–4522.

Conte, M.H., Dickey, T.D., Weber, J.C., Johnson, R.J., Knap, A.H., 2003. Transient physical forcing of pulsed export of bioreactive material to the deep Sargasso Sea. Deep Sea Research Part I: Oceanographic Research Papers 50 (10), 1157–1187.

Cuvelier, D., Ribeiro, P.A., Ramalho, S.P., Kersken, D., Martinez Arbizu, P., Colaço, A., 2020. Are seamounts refuge areas for fauna from polymetallic nodule fields? Biogeosciences 17 (9), 2657–2680.

d'Udekem d'Acoz, C., Havermans, C., 2015. Contribution to the systematics of the genus Eurythenes S.I. Smith in Scudder, 1882 (Crustacea: Amphipoda: Lysianassoidea: Eurytheneidae). Zootaxa 3971 (1).

Dahlgren, T., Wiklund, H., Rabone, M., Amon, D., Ikebe, C., Watling, L., Smith, C., Glover, A., 2016. Abyssal fauna of the UK-1 polymetallic nodule exploration area, Clarion-Clipperton Zone, central Pacific Ocean: Cnidaria. Biodiversity Data Journal 4, e9277.

Drazen, J.C., Leitner, A.B., Jones, D.O.B., Simon-Lledó, E., 2021. Regional variation in communities of demersal fishes and scavengers across the Clarion Clipperton Zone. Frontiers in Marine Science, section Deep-Sea Environments and Ecology.

Drazen, J.C., Phleger, C.F., Guest, M.A., Nichols, P.D., 2008. Lipid, sterols and fatty acid composition of abyssal holothurians and ophiuroids from the North-East Pacific Ocean: Food web implications. Comparative Biochemistry and Physiology Part B: Biochemistry and Molecular Biology 151 (1), 79–87.

Durden, J.M., Simon-Lledo, E., Gooday, A.J., Jones, D.O.B., 2017. Abundance and morphology of Paleodictyon nodosum, observed at the Clarion-Clipperton Zone. Marine Biodiversity 1–5.

Easton, E.E., Thistle, D., 2016. Do some deep-sea, sediment-dwelling species of harpacticoid copepods have 1000-km-scale range sizes? Molecular Ecology 25 (17), 4301–4318.

Fang, J., Kato, C., Sato, T., Chan, O., McKay, D., 2004. Biosynthesis and dietary uptake of polyunsaturated fatty acids by piezophilic bacteria. Comp Biochem Physiol B Biochem Mol Biol 137 (4), 455–461.

Fang, J., Uhle, M., Billmark, K., Bartlett, D.H., Kato, C., 2006. Fractionation of carbon isotopes in biosynthesis of fatty acids by a piezophilic bacterium Moritella japonica strain DSK1. Geochimica Et Cosmochimica Acta 70 (7), 1753–1760.

Gagosian, R.B., Peltzer, E.T., 1986. The importance of atmospheric input of terrestrial organic material to deep sea sediments. Organic Geochemistry 10 (4), 661–669.

Gazis, I.Z., Schoening, T., Alevizos, E., Greinert, J., 2018. Quantitative mapping and predictive modeling of Mn nodules' distribution from hydroacoustic and optical AUV data linked by random forests machine learning. Biogeosciences 15 (23), 7347–7377.
GEBCO, 2014. The GEBCO_2014 Grid, version 20141103, http://www.gebco.net.
Gillan, F.T., Johns, R.B., 1986. Chemical markers for marine bacteria: fatty acids and pigments. In: Johns, R.B. (Ed.), Biological Markers in the Sedimentary Environment. Elsevier Press, New York, pp. 291–309.
Glover, A., Dahlgren, T., Wiklund, H., Mohrbeck, I., Smith, C., 2016a. An End-to-End DNA Taxonomy Methodology for Benthic Biodiversity Survey in the Clarion-Clipperton Zone, Central Pacific Abyss. Journal of Marine Science and Engineering 4 (1), 2.
Glover, A., Wiklund, H., Rabone, M., Amon, D., Smith, C., O'Hara, T., Mah, C., Dahlgren, T., 2016b. Abyssal fauna of the UK-1 polymetallic nodule exploration claim, Clarion-Clipperton Zone, central Pacific Ocean: Echinodermata. Biodiversity Data Journal 4, e7251.
Glover, A.G., Smith, C.R., Paterson, G.L.J., Wilson, G.D.F., Hawkins, L., Sheader, M., 2002. Polychaete species diversity in the central Pacific abyss: local and regional patterns, and relationships with productivity. Marine Ecology Progress Series 240, 157–169.
Gooday, A., Goineau, A., Voltski, I., 2015. Abyssal foraminifera attached to polymetallic nodules from the eastern Clarion Clipperton Fracture Zone: a preliminary description and comparison with North Atlantic dropstone assemblages. Marine Biodiversity 1–22.
Gooday, A.J., Durden, J.M., Holzmann, M., Pawlowski, J., Smith, C.R., 2020a. Xenophyophores (Rhizaria, Foraminifera), including four new species and two new genera, from the western Clarion-Clipperton Zone (abyssal equatorial Pacific). European Journal of Protistology 75, 125715.
Gooday, A.J., Durden, J.M., Smith, C.R., 2020b. Giant, highly diverse protists in the abyssal Pacific: vulnerability to impacts from seabed mining and potential for recovery. Communicative & Integrative Biology 13 (1), 189–197.
Gooday, A.J., Holzmann, M., Caulle, C., Goineau, A., Jones, D.O.B., Kamenskaya, O., Simon-Lledó, E., Weber, A.A.T., Pawlowski, J., 2017a. New species of the xenophyophore genus Aschemonella (Rhizaria: Foraminifera) from areas of the abyssal eastern Pacific licensed for polymetallic nodule exploration. Zoological Journal of the Linnean Society 182 (3), 479–499.
Gooday, A.J., Holzmann, M., Goineau, A., Kamenskaya, O., Melnik, V.F., Pearce, R.B., Weber, A.A.T., Pawlowski, J., 2018. Xenophyophores (Rhizaria, Foraminifera) from the Eastern Clarion-Clipperton Zone (equatorial Pacific): the Genus Psammina. Protist 169 (6), 926–957.
Gooday, A.J., Holzmann, M., Goineau, A., Pearce, R.B., Voltski, I., Weber, A.A.T., Pawlowski, J., 2017b. Five new species and two new genera of xenophyophores (Foraminifera: Rhizaria) from part of the abyssal equatorial Pacific licensed for polymetallic nodule exploration. Zoological Journal of the Linnean Society 183 (4), 723–774.
Halbach, P., Rehm, E., Marchig, V., 1979. Distribution of Si, Mn, Fe, Ni, Cu Co, Zn, Pb, Mg, and Ca in grain-size fractions of sediment samples from a manganese nodule field in the Central Pacific Ocean. Marine Geology 29 (1), 237–252.
Havermans, C., 2016. Have we so far only seen the tip of the iceberg? Exploring species diversity and distribution of the giant amphipod Eurythenes. Biodiversity 17 (1–2), 12–25.
Havermans, C., Sonet, G., d'Udekem d'Acoz, C., Nagy, Z.T., Martin, P., Brix, S., Riehl, T., Agrawal, S., Held, C., 2013. Genetic and Morphological Divergences in the Cosmopolitan Deep-Sea Amphipod Eurythenes gryllus Reveal a Diverse Abyss and a Bipolar Species. PLoS ONE 8 (9), e74218.
Haxby, W.F., Weissel, J.K., 1986. Evidence for small-scale mantle convection from Seasat altimeter data. Journal of Geophysical Research: Solid Earth 91 (B3), 3507–3520.
Hayes, S.P., 1979. Benthic current observations at DOMES sites A, B, and C in the tropical North Pacific Ocean. In: Bischoff, J.L., Piper, D.Z. (Eds.), Marine Geology and Oceanography of the Pacific Manganese Nodule Province. Marine Science, New York, pp. 83–112.
Hayes, S.P., 1980. The Bottom Boundary Layer in the Eastern Tropical Pacific. Journal of Physical Oceanography 10 (3), 315–329.
Heezen, B.C., Hollister, C.D., 1971. The Face of the Deep. Oxford University Press, London.
Hein, J.R., Mizell, K., Koschinsky, A., Conrad, T.A., 2013. Deep-ocean mineral deposits as a source of critical metals for high- and green-technology applications: Comparison with land-based resources. Ore Geology Reviews 51, 1–14.
Hessler, R.R., Jumars, P.A., 1974. Abyssal community analysis from replicate box cores in the central North Pacific. Deep Sea Res. Oceanogr. Abstr 21 (3), 185–209.
Hollingsworth, A.L., Jones, D.O.B., Young, C.R., 2021. Spatial Variability of Abyssal Nitrifying Microbes in the North-Eastern Clarion-Clipperton Zone. Frontiers in Marine Science 8 (1023). https://doi.org/10.3389/fmars.2021.663420.
Horton, T., Cooper, H., Vlierboom, R., Thurston, M., Hauton, C., Young, C.R., 2020a. Molecular phylogenetics of deep-sea amphipods (Eurythenes) reveal a new undescribed species at the Porcupine Abyssal Plain, North East Atlantic Ocean. Progress in Oceanography 183, 102292.
Horton, T., Marsh, L., Bett, B.J., Gates, A.R., Jones, D.O.B., Benoist, N.M.A., Pfeifer, S., Simon-Lledó, E., Durden, J.M., Vandepitte, L., Appeltans, W., 2021. Recommendations for the Standardisation of Open Taxonomic Nomenclature for Image-Based Identifications. Frontiers in Marine Science 8 (62). https://doi.org/10.3389/fmars.2021.620702.
Horton, T., Thurston, M.H., Vlierboom, R., Gutteridge, Z., Pebody, C.A., Gates, A.R., Bett, B.J., 2020b. Are abyssal scavenging amphipod assemblages linked to climate cycles? Progress in Oceanography 184, 102318.
Howell, K.L., Pond, D.W., Billett, D.S.M., Tyler, P.A., 2003. Feeding ecology of deep-sea seastars (Echinodermata: Asteroidea): A fatty-acid biomarker approach. Marine Ecology Progress Series 255, 193–206.
International Seabed Authority, 2010. A geological model of polymetallic nodule deposits in the Clarion Clipperton Fracture Zone. Technical Study: No. 6. International Seabed Authority, Kingston, Jamaica. https://isa.org.jm/files/files/documents/tstudy6.pdf.
International Seabed Authority, 2011. Environmental Management Plan for the Clarion Clipperton Zone. ISBA/17/LTC/7. International Seabed Authority, Kingston, Jamaica. https://www.isa.org.jm/documents/isba17ltc7.
International Seabed Authority, 2020. Workshop Report: Deep CCZ Biodiversity Synthesis Workshop Friday Harbor, Washington, USA, 1-4 October 2019. Kingston, Jamaica. https://www.isa.org.jm/files/files/documents/Deep%20CCZ%20Biodiversity%20Synthesis%20Workshop%20Report%20-%20Final-for%20posting-clean-1.pdf.
Janssen, A., Kaiser, S., Meißner, K., Brenke, N., Menot, L., Martínez Arbizu, P., 2015. A Reverse Taxonomic Approach to Assess Macrofaunal Distribution Patterns in Abyssal Pacific Polymetallic Nodule Fields. PLoS ONE 10 (2), e0117790.
Janssen, A., Stuckas, H., Vink, A., Arbizu, P.M., 2019. Biogeography and population structure of predominant macrofaunal taxa (Annelida and Isopoda) in abyssal polymetallic nodule fields: implications for conservation and management. Marine Biodiversity 49 (6), 2641–2658.
Jeffreys, R.M., Wolff, G.A., Cowie, G.L., 2009a. Influence of oxygen on heterotrophic reworking of sedimentary lipids at the Pakistan margin. Deep Sea Research Part II: Topical Studies in Oceanography 56 (6), 358–375.
Jeffreys, R.M., Wolff, G.A., Murty, S.J., 2009b. The trophic ecology of key megafaunal species at the Pakistan Margin: Evidence from stable isotopes and lipid biomarkers. Deep-Sea Research Part I-Oceanographic Research Papers 56 (10), 1816–1833.
Jeong, K.S., Kang, J.K., Chough, S.K., 1994. Sedimentary processes and manganese nodule formation in the Korea Deep Ocean Study (KODOS) area, western part of Clarion-Clipperton fracture zones, northeast equatorial Pacific. Marine Geology 122 (1), 125–150.
Johnson, G.C., Toole, J.M., 1993. Flow of deep and bottom waters in the Pacific at 10°N. Deep Sea Research Part I: Oceanographic Research Papers 40 (2), 371–394.
Jones, D.O.B., all, 2015. RRS James Cook Cruise JC120 15 Apr - 19 May 2015. Manzanillo to Manzanillo, Mexico. Managing Impacts of Deep-seA resource exploitation (MIDAS): Clarion-Clipperton Zone North Eastern Area of Particular Environmental Interest (National Oceanography Centre Cruise Report 32). National Oceanography Centre, Southampton, p. 117.
Jones, D.O.B., Kaiser, S., Sweetman, A.K., Smith, C.R., Menot, L., Vink, A., Trueblood, D., Greinert, J., Billett, D.S.M., Arbizu, P.M., Radziejewska, T., Singh, R., Ingole, B., Stratmann, T., Simon-Lledó, E., Durden, J.M., Clark, M.R., 2017. Biological responses to disturbance from simulated deep-sea polymetallic nodule mining. PLoS ONE 12 (2), e0171750.
Juan, C., Van Rooij, D., De Bruycker, W., 2018. An assessment of bottom current controlled sedimentation in Pacific Ocean abyssal environments. Marine Geology 403, 20–33.
Jung, H.-S., Lee, C.-B., Jeong, K.-S., Kang, J.-K., 1998. Geochemical and mineralogical characteristics in two-color core sediments from the Korea Deep Ocean Study (KODOS) area, northeast equatorial Pacific. Marine Geology 144 (4), 295–309.
Kamenskaya, O.E., Melnik, V.F., Gooday, A.J., 2013. Giant protists (xenophyophores and komokiaceans) from the Clarion-Clipperton ferromanganese nodule field (eastern Pacific). Biology Bulletin Reviews 3 (5), 388–398.
Kawabe, M., Fujio, S., 2010. Pacific ocean circulation based on observation. Journal of Oceanography 66 (3), 389–403.
Kawamura, K., Ishimura, Y., Yamazaki, K., 2003. Four years' observations of terrestrial lipid class compounds in marine aerosols from the western North Pacific. Global Biogeochemical Cycles 17 (1), 3-1-3-19.
Kersten, O., Smith, C.R., Vetter, E.W., 2017. Abyssal near-bottom dispersal stages of benthic invertebrates in the Clarion-Clipperton polymetallic nodule province. Deep Sea Research Part I: Oceanographic Research Papers 127, 31–40.
Khripounoff, A., Caprais, J.-C., Crassous, P., Etoubleau, J., 2006. Geochemical and biological recovery of the disturbed seafloor in polymetallic nodule fields of the Clipperton-Clarion Fracture Zone (CCFZ) at 5,000-m depth. Limnology and Oceanography 51 (5), 2033–2041.
Kiriakoulakis, K., Bett, B.J., White, M., Wolff, G.A., 2004. Organic biogeochemistry of the Darwin Mounds, a deep-water coral ecosystem, of the NE Atlantic. Elsevier Science B.V, Amsterdam.
Koch, H., Lücker, S., Albertsen, M., Kitzinger, K., Herbold, C., Spieck, E., Nielsen, P.H., Wagner, M., Daims, H., 2015. Expanded metabolic versatility of ubiquitous nitrite-oxidizing bacteria from the genus Nitrospira. Proceedings of the National Academy of Sciences 112 (36), 11371-11376.
Könneke, M., Bernhard, A.E., de la Torre, J.R., Walker, C.B., Waterbury, J.B., Stahl, D.A., 2005. Isolation of an autotrophic ammonia-oxidizing marine archaeon. Nature 437 (7058), 543–546.
Kontar, E.A., Sokov, A.V., 1994. A benthic storm in the northeastern tropical Pacific over the fields of manganese nodules. Deep Sea Research Part I: Oceanographic Research Papers 41 (7), 1069–1089.
Kontar, E.A., Sokov, A.V., Demidova, T.A., Belyaev, A.M., 1994. Measurement of near-bottom currents on hills in the eastern equatorial Pacific Ocean. Proceedings of OCEANS'94, Brest, France, pp. 672-677.
Langenkämper, D., Zurowietz, M., Schoening, T., Nattkemper, T.W., 2017. BIIGLE 2.0 - Browsing and Annotating Large Marine Image Collections. Frontiers in Marine. Science 4 (83).

Laroche, O., Kersten, O., Smith, C.R., Goetze, E., 2020. From Sea Surface to Seafloor: A Benthic Allochthonous eDNA Survey for the Abyssal Ocean. Frontiers in Marine Science 7 (682).
Leitner, A.B., Neuheimer, A.B., Donlon, E., Smith, C.R., Drazen, J.C., 2017. Environmental and bathymetric influences on abyssal bait-attending communities of the Clarion Clipperton Zone. Deep Sea Research Part I: Oceanographic Research Papers 125 (Supplement C), 65–80.
Leitner, A.B., Neuheimer, A.B., Drazen, J.C., 2020. Evidence for long-term seamount-induced chlorophyll enhancements. Scientific Reports 10 (1), 12729.
Lim, S.-C., Wiklund, H., Glover, A.G., Dahlgren, T.G., Tan, K.-S., 2017. A new genus and species of abyssal sponge commonly encrusting polymetallic nodules in the Clarion-Clipperton Zone. East Pacific Ocean. Systematics and Biodiversity 15 (6), 507–519.
Lindh, M.V., Maillot, B.M., Shulse, C.N., Gooday, A.J., Amon, D.J., Smith, C.R., Church, M.J., 2017. From the Surface to the Deep-Sea: Bacterial Distributions across Polymetallic Nodule Fields in the Clarion-Clipperton Zone of the Pacific Ocean. Frontiers in Microbiology 8 (1696).
Lodge, M., Johnson, D., Le Gurun, G., Wengler, M., Weaver, P., Gunn, V., 2014. Seabed mining: International Seabed Authority environmental management plan for the Clarion-Clipperton Zone. A partnership approach. Marine Policy 49, 66–72.
Lodge, M.W., Segerson, K., Squires, D., 2017. Sharing and Preserving the Resources in the Deep Sea: Challenges for the International Seabed Authority. International Journal of Marine and Coastal Law 32 (3), 427–457.
Mansour, M.P., Holdsworth, D.G., Forbes, S.E., Macleod, C.K., Volkman, J.K., 2005. High contents of 24:6(n-3) and 20:1(n-13) fatty acids in the brittle star Amphiura elandiformis from Tasmanian coastal sediments. Biochemical Systematics and Ecology 33 (7), 659–674.
Marsh, L., Huvenne, V.A.I., Jones, D.O.B., 2018. Geomorphological evidence of large vertebrates interacting with the seafloor at abyssal depths in a region designated for deep-sea mining. Royal Society Open Science 5 (8), 180286.
McDougall, T., Feistel, R., Millero, F., Jackett, D.R., Wright, D., King, B., Marion, G., Chen, C.-T.A., Spitzer, P., 2010. The International Thermodynamic Equation of Seawater 2010 (TEOS-10): Calculation and Use of Thermodynamic Properties. Intergovernmental Oceanographic Commission (IOC) of UNESCO.
McQuaid, K.A., Attrill, M.J., Clark, M.R., Cobley, A., Glover, A.G., Smith, C.R., Howell, K. L., 2020. Using Habitat Classification to Assess Representativity of a Protected Area Network in a Large, Data-Poor Area Targeted for Deep-Sea Mining. Frontiers in Marine Science 7 (1066).
Menendez, A., James, R.H., Lichtschlag, A., Connelly, D., Peel, K., 2019. Controls on the chemical composition of ferromanganese nodules in the Clarion-Clipperton Fracture Zone, eastern equatorial Pacific. Marine Geology 409, 1–14.
Mewes, K., Mogollón, J.M., Picard, A., Rühlemann, C., Kuhn, T., Nöthen, K., Kasten, S., 2014. Impact of depositional and biogeochemical processes on small scale variations in nodule abundance in the Clarion-Clipperton Fracture Zone. Deep Sea Research Part I: Oceanographic Research Papers 91, 125–141.
Meyers, P.A., Leenheer, M.J., Eaoie, B.J., Maule, S.J., 1984. Organic geochemistry of suspended and settling particulate matter in Lake Michigan. Geochimica Et Cosmochimica Acta 48 (3), 443–452.
Mohrbeck, I., Horton, T., Jażdżewska, A.M., Martínez Arbizu, P., 2021. DNA-barcoding and Cryptic Diversity of Deep-Sea Scavenging Amphipods in the Clarion-Clipperton Zone (Eastern Equatorial Pacific).
Müller, P.J., 1977. CN ratios in Pacific deep-sea sediments: Effect of inorganic ammonium and organic nitrogen compounds sorbed by clays. Geochimica Et Cosmochimica Acta 41 (6), 765–776.
Mullineaux, L.S., 1987. Organisms living on manganese nodules and crusts: distribution and abundance at three North Pacific sites. Deep-Sea Research 34, 165–184.
Murray, J., Renard, A.F., 1891. Report on Deep-Sea Deposits based on the specimens collected during the voyage of H.M.S. Challenger in the years 1872 to 1876. Report on the scientific results of the voyage of H.M.S. Challenger during the years 1873-76.
Neto, R.R., Wolff, G.A., Billett, D.S.M., Mackenzie, K.L., Thompson, A., 2006. The influence of changing food supply on the lipid biochemistry of deep-sea holothurians. Deep Sea Research Part I: Oceanographic Research Papers 53 (3), 516–527.
Ohkouchi, N., Kawamura, K., Kawahata, H., Taira, A., 1997. Latitudinal distributions of terrestrial biomarkers in the sediments from the Central Pacific. Geochimica Et Cosmochimica Acta 61 (9), 1911–1918.
Ourisson, G., Rohmer, M., 1992. Hopanoids. 2. Biohopanoids: a novel class of bacterial lipids. Accounts of Chemical Research 25 (9), 403-408.
Paterson, G.L.J., Wilson, G.D.F., Cosson, N., Lamont, P.A., 1998. Hessler and Jumars (1974) revisited: abyssal polychaete assemblages from the Atlantic and Pacific. Deep Sea Research Part II: Topical Studies in Oceanography 45 (1), 225–251.
Peukert, A., Schoening, T., Alevizos, E., Köser, K., Kwasnitschka, T., Greinert, J., 2018. Understanding Mn-nodule distribution and evaluation of related deep-sea mining impacts using AUV-based hydroacoustic and optical data. Biogeosciences 15 (8), 2525–2549.
Puerta, P., Johnson, C., Carreiro-Silva, M., Henry, L.-A., Kenchington, E., Morato, T., Kazanidis, G., Rueda, J.L., Urra, J., Ross, S., Wei, C.-L., González-Irusta, J.M., Arnaud-Haond, S., Orejas, C., 2020. Influence of Water Masses on the Biodiversity and Biogeography of Deep-Sea Benthic Ecosystems in the North Atlantic. Frontiers in Marine Science 7 (239).
Purser, A., Herr, H., Dreutter, S., Dorschel, B., Glud, R.N., Hehemann, L., Hoge, U., Jamieson, A.J., Linley, T.D., Stewart, H.A., Wenzhöfer, F., 2019. Depression chains in seafloor of contrasting morphology, Atacama Trench margin: a comment on Marsh et al. (2018). Royal Society Open Science 6 (3), 182053.
Quast, C., Pruesse, E., Yilmaz, P., Gerken, J., Schweer, T., Yarza, P., Peplies, J., Glöckner, F.O., 2012. The SILVA ribosomal RNA gene database project: improved data processing and web-based tools. Nucleic Acids Research 41 (D1), D590–D596.
Radziejewska, T., Stoyanova, V., 2000. Abyssal epibenthic megafauna of the Clarion-Clipperton area (NE Pacific): changes in time and space versus anthropogenic environmental disturbance. Oceanological Studies 29 (2), 83–101.
Rampen, S.W., Abbas, B.A., Schouten, S., Sinninghe Damste, J.S., 2010. A comprehensive study of sterols in marine diatoms (Bacillariophyta): Implications for their use as tracers for diatom productivity. Limnology and Oceanography 55 (1), 91–105.
Reinthaler, T., Salgado, X.A.Á., Alvarez, M., van Aken, H.M., Herndl, G.J., 2013. Impact of water mass mixing on the biogeochemistry and microbiology of the Northeast Atlantic Deep Water. Global Biogeochemical Cycles 27 (4), 1151–1162.
Renaud-Mornant, J., Gourbault, N., 1990. Evaluation of abyssal meiobenthos in the eastern central Pacific (Clarion-Clipperton fracture zone). Progress in Oceanography 24 (1–4), 317–329.
Reuss, N., Poulsen, L., 2002. Evaluation of fatty acids as biomarkers for a natural plankton community. A field study of a spring bloom and a post-bloom period off West Greenland. Marine Biology 141 (3), 423–434.
Reykhard, L.Y., Shulga, N.A., 2019. Fe-Mn nodule morphotypes from the NE Clarion-Clipperton Fracture Zone, Pacific Ocean: Comparison of mineralogy, geochemistry and genesis. Ore Geology Reviews 110, 102933.
Riech, V., von Grafenstein, R., 1987. Sedimentological and geochemical trends in deep-sea sedimentation of the Clarion-Clipperton block southeast of Hawaii since the early Miocene. In: von Stackelberg, U., Beiersdorf, H. (Eds.), Manganese Nodules and Sediments in the Equatorial North Pacific Ocean. "Sonne" Cruise SO 25. Geologisches Jahrbuch Reihe D, Band D 87, Hannover.
Riehl, T., Wölfl, A.-C., Augustin, N., Devey, C.W., Brandt, A., 2020. Discovery of widely available abyssal rock patches reveals overlooked habitat type and prompts rethinking deep-sea biodiversity. Proceedings of the National Academy of Sciences, 201920706.
Ritchie, H., Jamieson, A.J., Piertney, S.B., 2015. Phylogenetic relationships among hadal amphipods of the Superfamily Lysianassoidea: Implications for taxonomy and biogeography. Deep Sea Research Part I: Oceanographic Research Papers 105, 119–131.
Rühlemann, C., Baumann, L., Blöthe, M., Bruns, A., Eisenhauer, A., Georgens, R., Hansen, J.L.S., Heuer, L., Kasten, S., Kuhn, T., 2010. Cruise report SO-205 Mangan - Microbiology, paleoceanography and biodiversity in the manganese nodule belt of the Equatorial NE Pacific - Papeete, Tahiti-Manzanillo, Mexico, 14 April - 21 May 2010. Bundesanstalt für Geowissenschaften und Rohstoffe, Hannover, p. 112.
Rühlemann, C., Kuhn, T., Wiedicke, M., Kasten, S., Mewes, K., Picard, A., 2011. Current Status of Manganese Nodule Exploration in the German License Area. Proceedings of the Ninth (2011) ISOPE Ocean Mining Symposium, June 19-24, 2011, Maui, Hawaii, USA. , pp. 168-173.
Santos, V., Billett, D.S.M., Rice, A.L., Wolff, G.A., 1994. Organic matter in deep-sea sediments from the Porcupine Abyssal Plain in the North-east Atlantic Ocean. 1. Lipids. Deep-Sea Research Part I: Oceanographic Research Papers 41 (5–6), 787–819.
Schneider, C.A., Rasband, W.S., Eliceiri, K.W., 2012. NIH Image to ImageJ: 25 years of image analysis. Nature Methods 9 (7), 671–675.
Schoening, T., Jones, D.O.B., Greinert, J., 2017. Compact-Morphology-based poly-metallic Nodule Delineation. Scientific Reports 7 (1), 13338.
Shulga, N.A., 2017. Distribution of n-alkanes in the ferromanganese nodule–sediment–pore water system (Clarion–Clipperton Fracture Zone). Lithology and Mineral Resources 52 (6), 435–441.
Shulga, N.A., 2018. Characteristics of Alkanes in Ferromanganese Nodules of the Clarion-Clipperton Fracture Zone. Oceanology 58 (5), 672–678.
Shulse, C.N., Maillot, B., Smith, C.R., Church, M.J., 2017. Polymetallic nodules, sediments, and deep waters in the equatorial North Pacific exhibit highly diverse and distinct bacterial, archaeal, and microeukaryotic communities. MicrobiologyOpen 6 (2), e00428.
Simon-Lledó, E., Bett, B.J., Huvenne, V.A.I., Schoening, T., Benoist, N.M.A., Jeffreys, R. M., Durden, J.M., Jones, D.O.B., 2019a. Megafaunal variation in the abyssal landscape of the Clarion Clipperton Zone. Progress in Oceanography 170, 119–133.
Simon-Lledó, E., Bett, B.J., Huvenne, V.A.I., Schoening, T., Benoist, N.M.A., Jones, D.O. B., 2019b. Ecology of a polymetallic nodule occurrence gradient: Implications for deep-sea mining. Limnology and Oceanography 64 (5), 1883–1894.
Simon-Lledó, E., Pomee, C., Ahokava, A., Drazen, J.C., Leitner, A.B., Flynn, A., Parianos, J., Jones, D.O.B., 2020. Multi-scale variations in invertebrate and fish megafauna in the mid-eastern Clarion Clipperton Zone. Progress in Oceanography 187, 102405.
Smith, C.R., Dahlgren, T.G., Drazen, J.C., Glover, A.G., Gooday, A., Kurras, G., Martinez-Arbizu, P., Shulse, C., Spickermann, R., Sweetman, A.K., Vetter, E., 2013. Abyssal Baseline Study (ABYSSLINE) Cruise Report.
Smith, C.R., Dahlgren, T.G., Drazen, J.C., Glover, A.G., Gooday, A., Kurras, G., Martinez-Arbizu, P., Shulse, C., Spickermann, R., Sweetman, A.K., Vetter, E., 2015a. Abyssal Baseline Study & Geophysical Survey (ABYSSLINE 02) Cruise Report.
Smith, C.R., De Leo, F.C., Bernardino, A.F., Sweetman, A.K., Arbizu, P.M., 2008. Abyssal food limitation, ecosystem structure and climate change. Trends in Ecology & Evolution 23 (9), 518–528.
Smith, C.R., et al., 2019. Deep CCZ Biodiversity Synthesis Workshop. Friday Harbor, Washington, USA, 1-4 October 2019. International Seabed Authority.
Smith, C.R., Glover, A.G., Treude, T., Higgs, N.D., Amon, D.J., 2015b. Whale-Fall Ecosystems: Recent Insights into Ecology, Paleoecology, and Evolution. Annual Review of Marine Science 7 (1), null.
Smith, C.R., Hoover, D.J., Doan, S.E., Pope, R.H., Demaster, D.J., Dobbs, F.C., Altabet, M. A., 1996. Phytodetritus at the abyssal seafloor across 10 degrees of latitude in the central equatorial Pacific. Deep-Sea Research Part II: Topical Studies in Oceanography 43 (4–6), 1309–1338.

Smith, C.R., Tunnicliffe, V., Colaço, A., Drazen, J.C., Gollner, S., Levin, L.A., Mestre, N.C., Metaxas, A., Molodtsova, T.N., Morato, T., Sweetman, A.K., Washburn, T., Amon, D. J., 2020. Deep-Sea Misconceptions Cause Underestimation of Seabed-Mining Impacts. Trends in Ecology & Evolution.

Soo, R.M., Skennerton, C.T., Sekiguchi, Y., Imelfort, M., Paech, S.J., Dennis, P.G., Steen, J.A., Parks, D.H., Tyson, G.W., Hugenholtz, P., 2014. An expanded genomic representation of the phylum cyanobacteria. Genome Biol Evol 6 (5), 1031–1045.

Taboada, S., Riesgo, A., Wiklund, H., Paterson, G.L.J., Koutsouveli, V., Santodomingo, N., Dale, A.C., Smith, C.R., Jones, D.O.B., Dahlgren, T.G., Glover, A. G., 2018. Implications of population connectivity studies for the design of marine protected areas in the deep sea: An example of a demosponge from the Clarion-Clipperton Zone. Molecular Ecology 27, 4657–4679.

Thomson, C.W., Murray, J., 1895. Report of the scientific results of the voyage of H.M.S. Challenger during the years 1873-76., London.

Thurston, M.H., 1990. Abyssal necrophagous amphipods (Crustacea: Amphipoda) in the northeast and tropical Atlantic Ocean. Progress in Oceanography 24 (1), 257–274.

Vanreusel, A., Hilario, A., Ribeiro, P.A., Menot, L., Arbizu, P.M., 2016. Threatened by mining, polymetallic nodules are required to preserve abyssal epifauna. Scientific Reports 6, 26808.

Veillette, J., Juniper, S.K., Gooday, A.J., Sarrazin, J., 2007a. Influence of surface texture and microhabitat heterogeneity in structuring nodule faunal communities. Deep Sea Research Part I: Oceanographic Research Papers 54 (11), 1936–1943.

Veillette, J., Sarrazin, J., Gooday, A.J., Galéron, J., Caprais, J.-C., Vangriesheim, A., Étoubleau, J., Christian, J.R., Kim Juniper, S., 2007b. Ferromanganese nodule fauna in the Tropical North Pacific Ocean: Species richness, faunal cover and spatial distribution. Deep Sea Research Part I: Oceanographic Research Papers 54 (11), 1912–1935.

Volz, J.B., Mogollón, J.M., Geibert, W., Arbizu, P.M., Koschinsky, A., Kasten, S., 2018. Natural spatial variability of depositional conditions, biogeochemical processes and element fluxes in sediments of the eastern Clarion-Clipperton Zone, Pacific Ocean. Deep Sea Research Part I: Oceanographic Research Papers 140, 159–172.

Wakeham, S.G., Hedges, J.I., Lee, C., Peterson, M.L., Hernes, P.J., 1997. Compositions and transport of lipid biomarkers through the water column and surficial sediments of the equatorial Pacific Ocean. Deep Sea Research Part II: Topical Studies in Oceanography 44 (9), 2131–2162.

Wakeham, S.G., Peterson, M.L., Hedges, J.I., Lee, C., 2002. Lipid biomarker fluxes in the Arabian Sea, with a comparison to the equatorial Pacific Ocean. Deep Sea Research Part II: Topical Studies in Oceanography 49 (12), 2265–2301.

Washburn, T.W., Jones, D.O.B., Wei, C.-L., Smith, C.R., 2021. Environmental Heterogeneity Throughout the Clarion-Clipperton Zone and the Potential Representativity of the APEI Network. Frontiers in Marine Science 8 (319).

Wear, E.K., Church, M.J., Orcutt, B.N., Shulse, C.N., Lindh, M.V., Smith, C.R., 2021. Bacterial and Archaeal Communities in Polymetallic Nodules, Sediments, and Bottom Waters of the Abyssal Clarion-Clipperton Zone: Emerging Patterns and Future Monitoring Considerations. Frontiers in Marine Science 8 (480).

Wedding, L.M., Friedlander, A.M., Kittinger, J.N., Watling, L., Gaines, S.D., Bennett, M., Hardy, S.M., Smith, C.R., 2013. From principles to practice: a spatial approach to systematic conservation planning in the deep sea. Proceedings of the Royal Society B: Biological Sciences 280 (1773), 20131684.

Wessel, P., Harada, Y., Kroenke, L.W., 2006. Toward a self-consistent, high-resolution absolute plate motion model for the Pacific. Geochemistry, Geophysics, Geosystems 7 (3), Q03L12.

Wigham, B.D., Hudson, I.R., Billett, D.S.M., Wolff, G.A., 2003. Is long-term change in the abyssal Northeast Atlantic driven by qualitative changes in export flux? Evidence from selective feeding in deep-sea holothurians. Progress in Oceanography 59 (4), 409–441.

Wijffels, S.E., Toole, J.M., Bryden, H.L., Fine, R.A., Jenkins, W.J., Bullister, J.L., 1996. The water masses and circulation at 10°N in the Pacific. Deep Sea Research Part I: Oceanographic Research Papers 43 (4), 501–544.

Wiklund, H., Neal, L., Glover, A.G., Drennan, R., Rabone, M., Dahlgren, T.G., 2019. Abyssal fauna of polymetallic nodule exploration areas, eastern Clarion-Clipperton Zone, central Pacific Ocean: Annelida: Capitellidae, Opheliidae, Scalibregmatidae, and Travisiidae. ZooKeys 883.

Wiklund, H., Taylor, J.D., Dahlgren, T.G., Todt, C., Ikebe, C., Rabone, M., Glover, A.G., 2017. Abyssal fauna of the UK-1 polymetallic nodule exploration area, Clarion-Clipperton Zone, central Pacific Ocean: Mollusca. ZooKeys 707, 1–46.

Winterer, E.L., Sandwell, D.T., 1987. Evidence from en-echelon cross-grain ridges for tensional cracks in the Pacific plate. Nature 329, 534.